National Central University

Department of Physics

Master's Thesis

Evaluation of position resolution and efficiency for GEM tracker in J-PARC E16 experiment

Graduate Student: Po-Hung Wang

Advisor: Wen-Chen Chang

October, 2023

Abstract

The J-PARC E16 experiment perform the collision of high-intensity 30-GeV proton beams with carbon, copper and nuclear targets, measure the mass spectra of light vector mesons which decay inside the nucleus. The experiment can help to understand the origin of hadron mass and the chiral symmetry. GEM tracker (GTR) is one of detector used for tracking in the experiment. Currently, the timing and position dependency on the GTRs' residual are observed, so the work of improved calibration is to eliminate the dependency and reduce the width of residual. We tune the Lorentz angle and offset constant in the hit positions of GTR used in reconstructing a track. The dependencies are eliminated successfully in the GTR100 and GTR200, but not for GTR300. After finishing the calibration work, the position resolutions and efficiencies of three GTRs inside the module 106 are evaluated for the commissioning run. The position resolutions of GTR100, 200 and 300 are determined to be 230 μm in x direction and 440 μm in y direction. It is good enough for track analysis but does not reach the requirement(100 μm in x direction). The efficiencies, in x direction, get 95% on GTR100 and 200, but only 88% on GTR300. In y direction, the improved of efficiency should be done because they are only 85%, 75% and 60% in respectively.

Acknowledgements

First of all, I would like to appreciate my advisor, Dr. Wen-Chen Chang. Thanks for giving a chance to join his group in two years ago so that I had a fulfilling life in my master study. He always gave me a lot of assistance when I faced any problems. I learned many physics knowledge, the method of dealing with problem, the ability to express something correctly, etc. I hope I have progressed in these days.

Secondly, I would like to express my gratitude to Dr. S. Yokkaichi, Dr. K. Ozawa and Dr. Y. Morino for the great help in many discussions. Thank Dr. S. Yokkaichi for providing the first training in the E16 so that I had a basic understanding for E16 experiment. Thank Dr. K. Ozawa for his patient explanation if I was confused by the discussion in the meeting. Thank Dr. Y. Morino for many support and advice in my analysis work. He helped me to clarify many problems.

Next, I would like to thanks to Mr. T. Murakami, Mr. M. Ichikawa and Ms. S. Nakasuga. They helped me a lot for the daily when I visited in Japan.

Then, I am truly grateful to my family. They gave me a tremendous support and encouragement so I can choose what I want. I also would like to express my appreciation to my friend, Kun-ni Liu. Thanks for her company and bringing a lot of fun in my life.

Finally, thanks everyone for all the help again.

Contents

List of Figures

List of Tables

Chapter 1

Introduction

1.1 Chiral system breaking in QCD

Quantum chromodynamics (QCD) is the theory of strong interaction, describing the properties of quarks and gluons. It is a qauge theory of the SU(3) group. One of the interesting feature of QCD is the spontaneous breaking of chiral symmetry, which can help understand the origin of hadron mass in low energy scale.

Chiral symmetry[1]
The quark part of Lagrangian of QCD is ,

$$\mathcal{L} = \overline{\Psi}_f(i\gamma^\mu D_\mu - m)\Psi_f$$

$$where,\ D_\mu = \partial_\mu + igA_\mu$$

One of symmetry can be considered in this Lagrangian may depend on the value of quark mass. The simplest model is the one which only contains two lightest quarks, u and d. If $m_u = m_d$, the Lagrangian would not change under flavor transformation,

$$\Psi_i \to (e^{i\vec{\alpha}\cdot\vec{\sigma}/2})_{ij}\Psi_j$$

so that the isospin is conversed. If the special case is considered, $m_u = m_d = 0$, the Lagrangian becomes,

$$\mathcal{L} = \overline{\Psi}_f(i\gamma^\mu D_\mu)\Psi_f$$

Here, the right-handed and left-handed property are introduced and can be written as,

$$\Psi_f = \begin{pmatrix} \psi_{fL} \\ \psi_{fR} \end{pmatrix} = \begin{pmatrix} \frac{1}{2}(1-\gamma^5)\psi_f \\ \frac{1}{2}(1+\gamma^5)\psi_f \end{pmatrix}$$

Putting them in the Lagrangian, the left-handed and right-handed quarks can be decoupled and operated separately. It is invariant if we transform the left-handed or right-handed system,

$$\psi_L \to e^{i\vec{\gamma}\cdot\vec{\sigma}/2}\psi_L,\ \psi_R \to e^{i\vec{\delta}\cdot\vec{\sigma}/2}\psi_R$$

$$Chiral\ group = SU_L(N_f) \otimes SU_L(N_f)$$

Therefore, the conclusion of chiral symmetry is that the rotation of left-handed and right-handed quarks would not change the Lagrangian.

Quark condensate[2]
The quark condensate is a vacuum expectation value of the composite operators from quark and anti-quark. The expectation value can be given like,

$$\langle \psi_i \bar{\psi}_j \rangle = \sigma \delta_{ij}$$

The σ is a constant and corresponding to the strong coupling scale Λ_{QCD}. The formation of quark condensate can be analogous to the pairs of electron condense in the ground state of a superconductor. The quark-antiquark pairs can be bound by strong interaction easily because of the confinement and the small mass of themselves. It is expected that the vacuum of QCD fill quark-antiquark pairs. Then the effective mass of u and d quarks are obtained by interacting with these bound states.

Symmetry breaking[3][4]
There are two breaking of chiral symmetries introduced in here. First one is "spontaneous" symmetry breaking, which means the Lagrangian is symmetric, but the ground state violates some symmetries in the system. In the case of chiral symmetry in QCD, The assumption of zero mass quarks make the Lagrangian is symmetric, but according to the discussion of quark condensate, the vacuum expectation value is not zero. Therefore, the spontaneous breaking of chiral symmetry appears, which is the spontaneous breaking of continuous symmetry. As Nambu-Goldstone theorem, there will be a massless particle produced, called the Goldstone boson. In chiral symmetry breaking, the π meson corresponds to the Goldstone boson. The other symmetry breaking is introduced, called "explicit" symmetry breaking. Because the mass of quarks are not zero actually, so the chiral symmetry is broken again in previous discussion. With this effect, the π meson has small masses as we know.

Based on the above information, it can be summarized as follows. In QCD, there is a exact chiral symmetry if quarks are massless. But, in the real world, quarks have the mass, even the lightest two quarks u and d (a few MeV/c^2), so the exact chiral symmetry is broken. Fortunately, the mass of light quarks are smaller than the QCD scale, it can be treated as a perturbation and the chiral symmetry is still regarded as a "approximated" symmetry. However, the QCD ground state is not a real "vacuum", it is characterized by the quark-antiquark pairs, which called the quark condensate $\langle q\bar{q} \rangle$, so the spontaneous breaking is occurred. This phenomenon explain why a hadron with large mass can consist of several light quarks.

Quark condensate is an order parameter relate to chiral symmetry, if $\langle q\bar{q} \rangle$=0, it is chiral symmetry phase, on the contrary, $\langle q\bar{q} \rangle$ is finite value, which means the chiral symmetry is broken. According to Fig. 1.1, $\langle q\bar{q} \rangle$ has a dependency on the temperature and density. At the lowest temperature and density, absolute value of $\langle q\bar{q} \rangle$ is maximum, and it decrease to zero until critical temperature or density[5]. Therefore, in an environment of finite temperature and density, the spontaneous chiral symmetry breaking remains, but it is restored partially.

Although $\langle q\bar{q} \rangle$ itself can't be observable and measured, there are several theoretical methods provided to study this topic[6][7][8]. One of them, for the chiral symmetry restoration in medium (finite density), QCD sum rule shows the relationship between mass spectrum and quark condensate and then it can be predicted the mass modification in different density environment like Fig. 1.2. The dependence is described by the linear equation $m(\rho)/m(0) = 1 - k_1(\rho/\rho_0)$, where k_1 is the parameter of shift. Namely, if the

density is confirmed, the decreasing of hadron mass can be known.

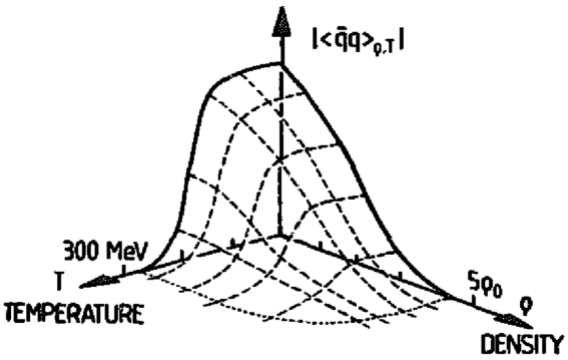

Figure 1.1: Correlation between quark condensate and temperature and density[1]

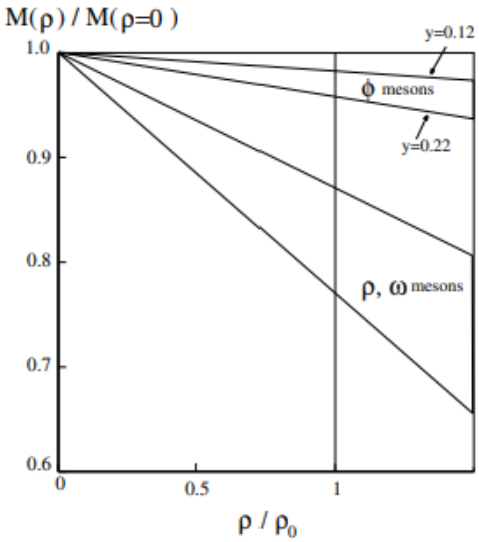

Figure 1.2: The mass modification of vector mesons as a function of ratio of density[7]

1.2 Previous experiment

There were several experiments investigating the modification of hadron mass in hot/dense matter. For example, CERES[9] and NA60[10] at CERN-SPS, KEK-PS E325[11], CLAS-G7 at JLab[12], etc. Table. 1.1 summarizes the results of these experiments except E325,

Table 1.1: The experiments about the mass modification

Experiment	Reaction	Environment	Measurement	Result
CERES	$Pb - Au$ collision	hot and dense	e^+e^- pairs	The modification of ρ meson is observed
NA60	$In - In$ collisions	hot and dense	$\mu^+\mu^-$ pairs	The mass spectrum of ρ meson is widen but no change in mass
CLAS-G7	$\gamma - D_2, C, Ti, Fe$	dense	e^+e^- pairs	The mass shift is small or even no exist and the width of ρ meson is unchanged

The KEK-PS E325 experiment, the predecessor of the J-PARC E16 experiment, measure the vector mesons mass in the nucleus. It is observed that the mass modification can be found in baryon density. An experiment was performed at KEK proton synchrotron, where 12 GeV proton hit the fixed carbon and copper targets. The spectrometer measured the electron-positron pair to reconstruct the invariant mass of vector mesons. The reaction process as follows,

$$p + C, Cu \rightarrow \rho, \omega, \phi \rightarrow e^+e^-$$

It is expected that slowly-moving vector mesons have high probability decaying inside the nuclear. These mesons cause the mass spectra getting wider in the low mass side and decrease the mass. The experiment uses two different targets (C and Cu) in order to investigate the nuclear size dependence of the mass spectra.

The following are the results from E325. As shown in the Fig. 1.3, there are significant excesses in the low side of mass near the ω mesons, as seen that the fitting result is not consistent with the data points. It is not caused by the background or model failure. The reason is that the mass modification hasn't been considered yet. Because of the short lifetime, ρ, ω mesons have a high probability of decaying in the nucleus. In Fig. 1.4, the range of invariant mass is the focus of ρ and ω mesons, the background has been subtracted and the ρ, ω mass modification are used in the fit. The fitting to data yields the result of shift parameter $k_1 = 0.092 \pm 0.002$

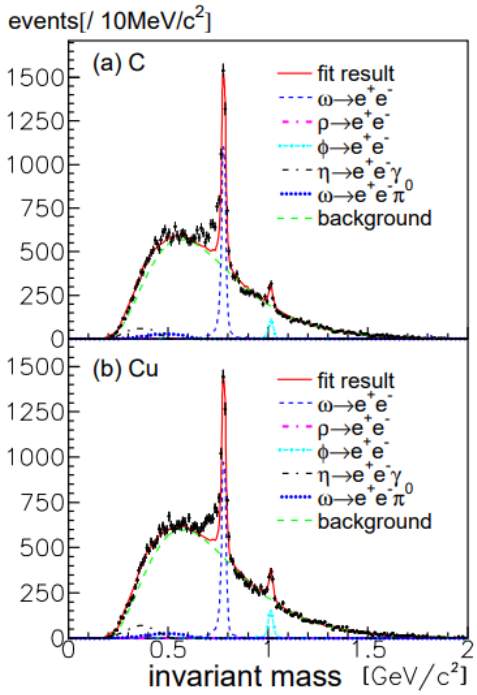

Figure 1.3: The invariant mass distribution of e^+e^- with many kind of decay channel and background[11]

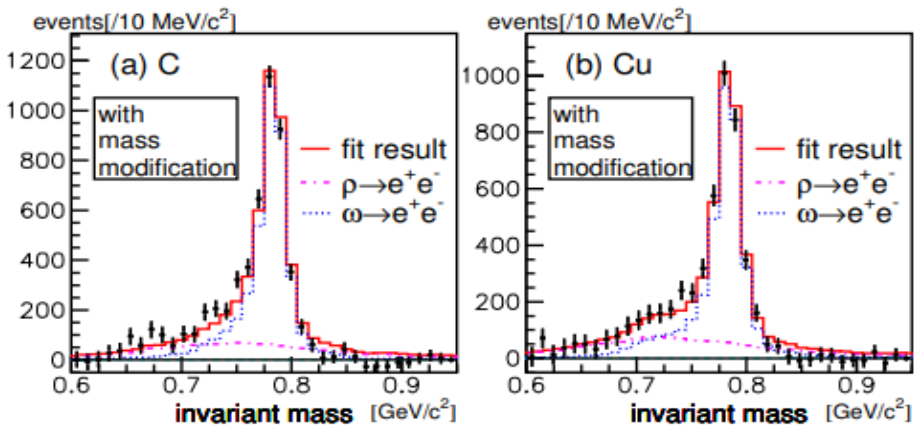

Figure 1.4: The fitting result of the invariant mass for ρ and ω mesons[11]

For the ϕ meson, whose mass modification is only observed in E325 experiment[13], the results are not only shown with two targets but also different $\beta\gamma$ in Fig. 1.5. Only those of slower velocity in the Cu target can be observed the significant excesses. The reason is that ϕ mesons have longer lifetime, so the probabilities of decaying inside the nucleus are lower than ρ and ω mesons.

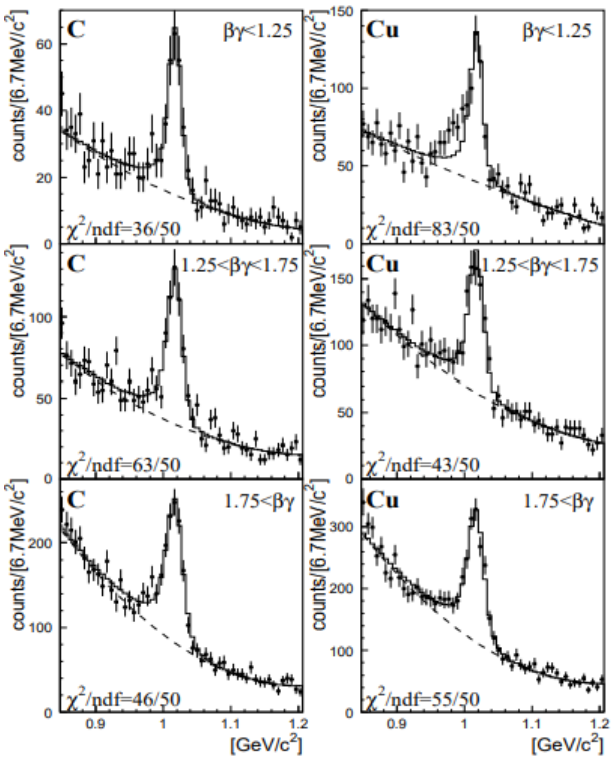

Figure 1.5: The invariant mass spectra of $\phi \to e^+e^-$[13]

The shortages of the E325 are the lack of statistics and high mass resolution, so even thought the mass modification in the experiment has been certain, it can not make a clear conclusion. The J-PARC E16 experiment, is planned to investigate these observation. The detail of E16 is explained in Chapter. 2.

Chapter 2

J-PARC E16 experiment

2.1 Overview

The E16 experiment aims to investigate the mass modification by measuring the mass spectra of light mesons in nucleus systematically. The experiment uses the high-flux 30-GeV proton beam to collide the fixed target in order to produce light vector mesons. It collects di-electron events from the decay of mesons to reconstruct the mass spectra. The $\phi \to e^+e^-$ is the particular channel in the experiment for helping to study hadron properties. The advantages of $\phi \to e^+e^-$ are as follows, (1) ϕ has a narrow mass spectra and there are no other mesons with similar mass. (2) the decay of e^+e^- has small final state interaction. While, there are also some disadvantages, (1) the statistic of ϕ mesons is low in $p+A$ interaction. (2) the branching ratio of $\phi \to e^+e^-$ is very small. Thankfully, these problems can be overcome by high intensity of proton beams delivered by J-PARC.

Compare to E325 experiment, in order to do the further systematic study and improve the statistic, E16 experiment uses a new beam line and construct a new spectrometer to achieve the 100 times statistics. The improvements are as follows,

- $10\times$ beam intensity
- $2\times$ cross section
- $5\times$ acceptance

Meanwhile, the new target selection is applied for confirming nuclear size dependence. With these enhancement, the experiment is expected to get the precise result in the invariant mass spectrum of e^+e^- like Fig. 2.1. The mass spectrum has distinctly two peak in the heavy nucleus with slow velocity. The peak at right hand side is for the ϕ mass which decay in free space and the other peak shows the ϕ decay inside nucleus.

For building the invariant mass, the identification of di-electron decay of ϕ mesons is required. The two electron track candidates are necessary. Each of them is selected by tracking and electron identified detectors which are introduced in later section. The opening angle for combination of two tracks is limited to a large angle to reject background electrons from π^0 Dalitz decay. The selection is relied on trigger and data acquisition system in the experiment.

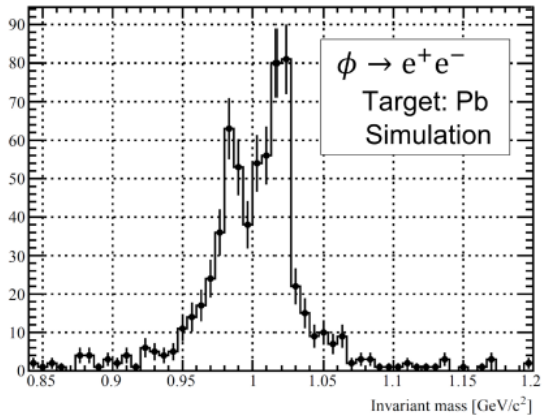

Figure 2.1: Monte Carlo simulation of the ϕ mass spectrum with $\beta\gamma$ less than 0.5 using Pb target

2.2 Experiment schedule

The E16 experiment has completed four stages of commissioning run and will start the physical run in the future. In Table. 2.1, it provides the detail for each run.

Table 2.1: schedule of the commissioning and physical run

Name	purpose	time	
Run0a	commissioning	2020/06/04	2020/06/20
Run0b	commissioning	2021/02/11	2021/02/18
Run0c	commissioning	2021/05/29	2021/06/09
Run0d	commissioning	2023/06/16	2023/06/22
Run1	physical data taking	unsure, next beam will be in 2024	
Run2	physical data taking	after the Run1	

2.3 Beam line

A high momentum proton beam used in E16 experiment is provided from the J-PARC's accelerator, which consist of three different accelerators. Proton beams are first accelerated to 400 MeV in a linear accelerator, then accelerated to 3 GeV in RCS, finally achieve to 30 GeV in the MR. The location of three accelerators are shown in Fig. 2.2. After that, the beams with high intensity 1×10^{10} proton/spill are extracted from MR and sent to the Hadron hall, where the spectrometer is located[16][17].

Figure 2.2: Accelerator structure of J-PARC

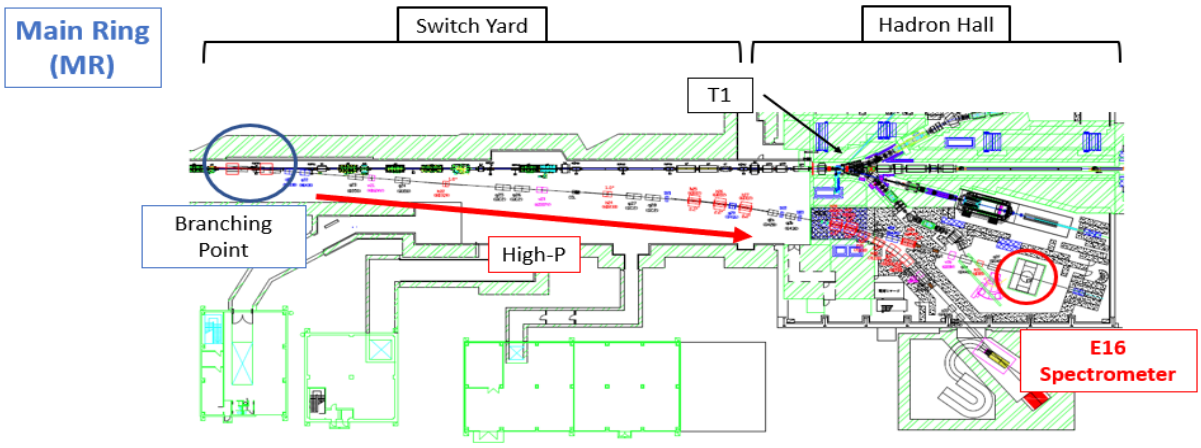

Figure 2.3: The beamline used for E16 experiment

2.4 Spectrometer

In E16 experiment, the spectrometer consists of four types detector surrounding the target which are placed at the center of the spectrometer magnet. The schematic view of a proposed spectrometer is shown in Fig. 2.4. There are one layer of silicon strip detectors (SSD) and three layers of GEM trackers (GTR) installed at inner region which used to track a particle trajectory. For electron identification, a hadron blind gas Cerenkov counters (HBD) and lead-glass EM calorimeters (LG) are covered at outer part.

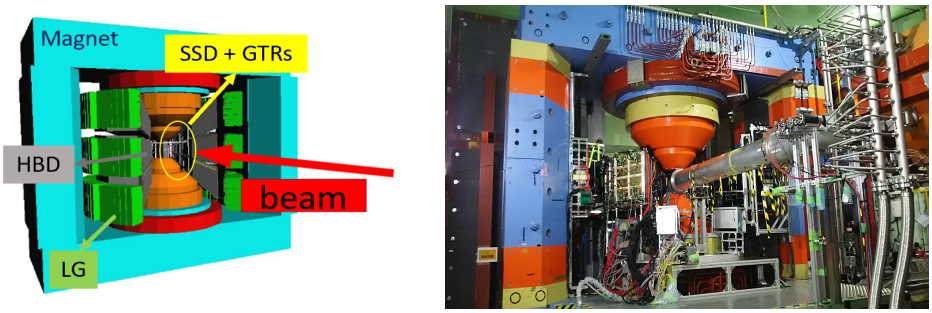

Figure 2.4: E16 spectrometer

In each run, there are different numbers of modules. One module is comprised of SSD, three layers of GTR, HBD and LG, covering the same acceptance in terms of polar angles. The modules are numbered from 101 to 109. The horizontal cross-section of module configuration is shown in Fig. 2.5a. Taking Run0c for example, the spectrometer is set up in the red line area. In order to avoid beam halo, there is no acceptance of small angle in the forward region. For physical run, Run1, detector will be upgraded and there will be 8 modules used to collect data. Furthermore, in Run2, the number of modules will be increased at upper and lower stages, total of 26 modules will be displayed. The module configuration is shown in Fig. 2.5b and its geometrical acceptance can be ±135° in horizontal and ±45° in vertical.

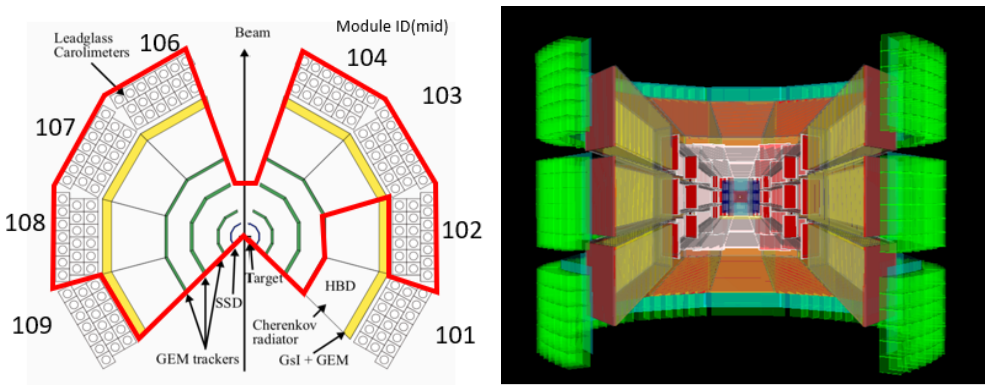

(a) the cross-section of middle stage (b) 3D view of spectrometer in Run2

Figure 2.5: Schematic view of the spectrometer

2.4.1 Target

Difference from E325, E16 experiment add two more targets, polyethylene (CH_2) and Pb. Pb is larger than Cu, which help to check the variety of mass modification in a heavier nuclear. The thickness of targets are also reselected. Although the thicker target can increase the number of interaction, the background of electron pair which produced from $\pi^0 \to \gamma\gamma$ are raised at the same time. In the commissioning run, there are two Cu and a C target used and the target from the upstream to downstream is Cu, C and Cu. The setting of targets are summarized in the Table. 2.2[19].

Table 2.2: Target of E325 and E16 commissioning run[19]

	nucleus	thickness (μm)	interaction length (%)	radiation length (%)
E325	C	810	0.21	0.43
	Cu	81	0.054	0.57
E16	C	500	0.10	0.21
	Cu	80	0.052	0.55

2.4.2 Silicon Strip Detector (SSD)

SSD is a position detector which are placed at the innermost of four tracking devices. It is composed of equidistant silicon strips. Since SSD have high spatial and timing resolution, it is expected that a better resolution of mass spectra can be obtained. In first three commissioning Runs, SSD have been installed on the spectrometer. The strips are only on the vertical orientation so the position information can be recorded on x direction. There is new SSD are prepared for next Run, which called the silicon tracking system (STS). This new detector can detect hits position in two dimension and further improve the resolution.

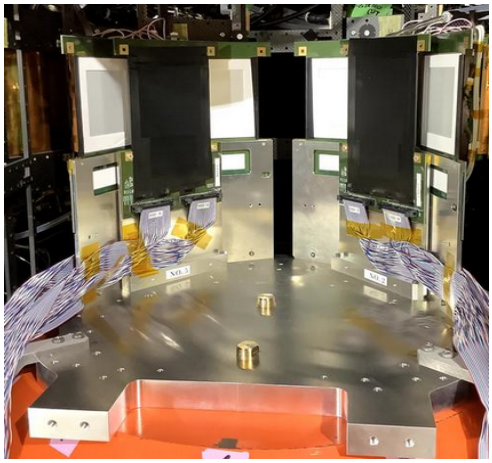

Figure 2.6: The photograph of SSD used in commissioning run

2.4.3 Gas Electron Multiplier Tracker (GTR)

There are three layers of GEM trackers, GTR100,GTR200 and GTR300 behind the SSD, which can measure the position of charged particle in two dimension. The areas are $100 \times 100\text{mm}^2$, $200 \times 200\text{mm}^2$, $300 \times 300\text{mm}^2$ respectively. Combined with the position of SSD, the trajectory of particle can be reconstructed. Using the curve of trajectory, information of magnetic filed, the momentum of charged particle can be calculated. The detail of GEM tracker is written in Section 2.5.

2.4.4 Hadron Blind Detector (HBD)

The major background event of the experiment is pions, in order to remove the background, the electron identified detector is required. HBD is a gas Cherenkov detector which design is a windowless and mirrorless structure. It consists of a gas radiator, GEMs and hexagonal readout board. The gas of CF_4 is not only used as the gas radiator, but also the amplification gas in GEMs.

Following is the working principle of HBD for distinguishing electron from others. When charged particle comes, only electrons can emit Cherenkov light in the radiator in the momentum region of interest, while pions can not. The light is converted to photoelectron by the CsI which is on the top of first stack of GEM. Then the photoelectron is subject to three times amplification and read out by the board. However, besides photonelectron induced by Cherenkov light, ionized electrons generated by a charged particle and gas can also induce signal. To avoid this case, an electric field is applied to detector between the mesh and first GEM to absorb these ionized electrons, the voltage configuration is called "reverse bias mode".

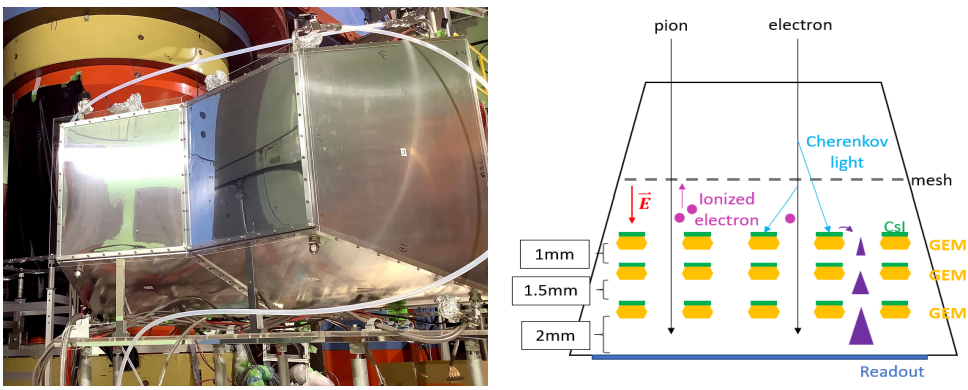

(a) The photograph of HBD gas vessel, they are used for two module

(b) The principle of particle identify of HBD

Figure 2.7: The photograph and schematic view of the HBD

2.4.5 Lead Glass Calorimeter (LG)

LG is a EM calorimeter made of a crystal and a photomultiplier. It is also used to differentiate electrons from pions. An electromagnetic shower is induced by a incident charged particles or photons then the light from the shower is detected by the photomultiplier. According to the amount of light, the electrons can be identified due to the number of photon is more than pions.

Figure 2.8: The photograph of LG

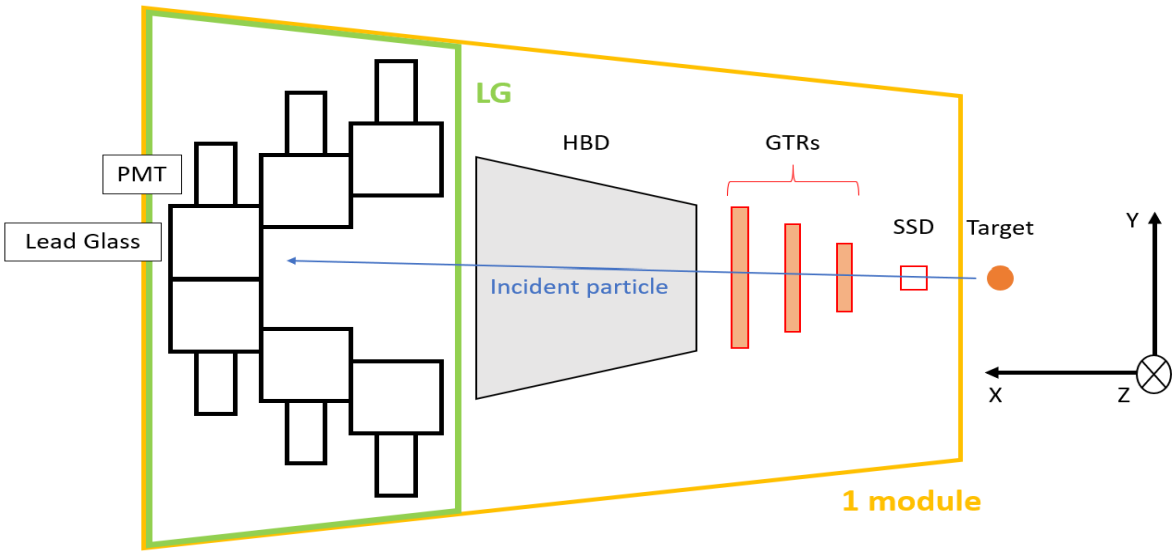

Figure 2.9: The schematic view of LG

2.5 GEM tracker

Fig. 2.10 is shown a photograph of three layers of GTR for a single module and electric circuit for three size of GTRs[20]. The design of three GTRs are different. A GTR consists of a mylar, a mesh, three GEM foils and a two-dimensional readout board. The chamber is filled with a gas mixed by Ar(70%) and CO_2(30%) which used to amplify a signal.

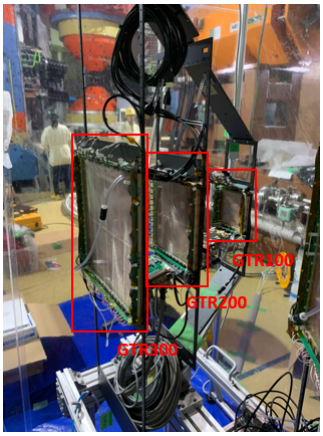

(a) The photograph of GTR

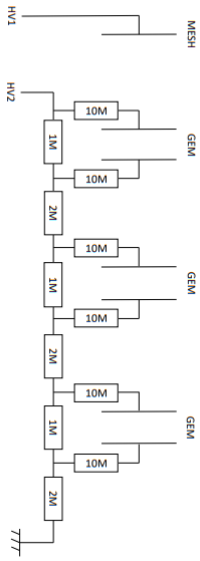

(b) The electric circuit of GTR100

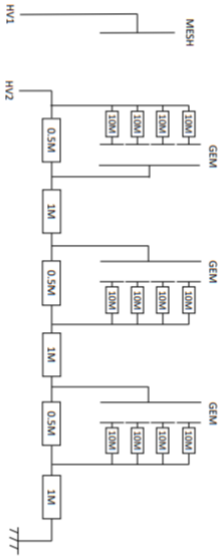

(c) The electric circuit of GTR200

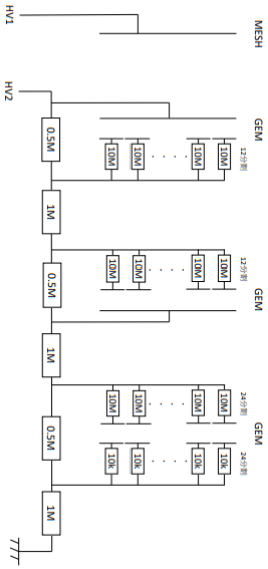

(d) The electric circuit of GTR300

Figure 2.10: The photograph and electric circuit of GTRs.

The principle of GTR is shown in Fig. 2.11. When charged particles enter a chamber, the gas is ionized to produce electrons. The ionized electrons are transported to the GEMs and readout board because of the electric field. They are multiplied by three GEM foils and then read out by two dimensional strips.

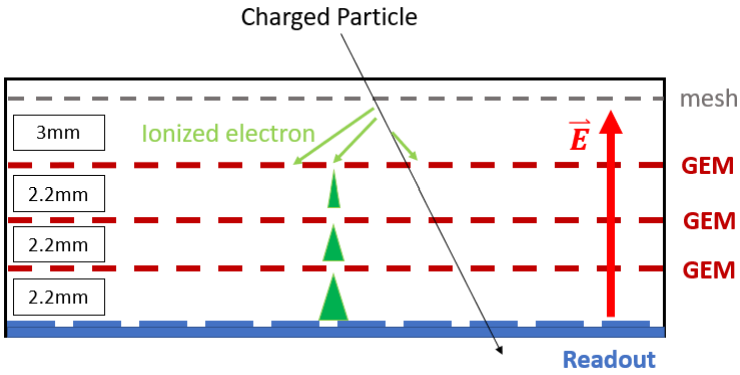

Figure 2.11: The principle of GTR

2.5.1 Gas Electron Multiplier

The gas electron multiplier consists of a thin insulator sandwiched by metal on the both sides. It has a high density of holes. GEM is placed between drift cathode plane (mesh) and readout board with applying high voltage . The voltage generates a strong electric field in each hole. Due to a strong electric field, ionized electrons can be amplified by electron avalanche. The more layers of GEMs are used, the higher gain can be achieved[21].

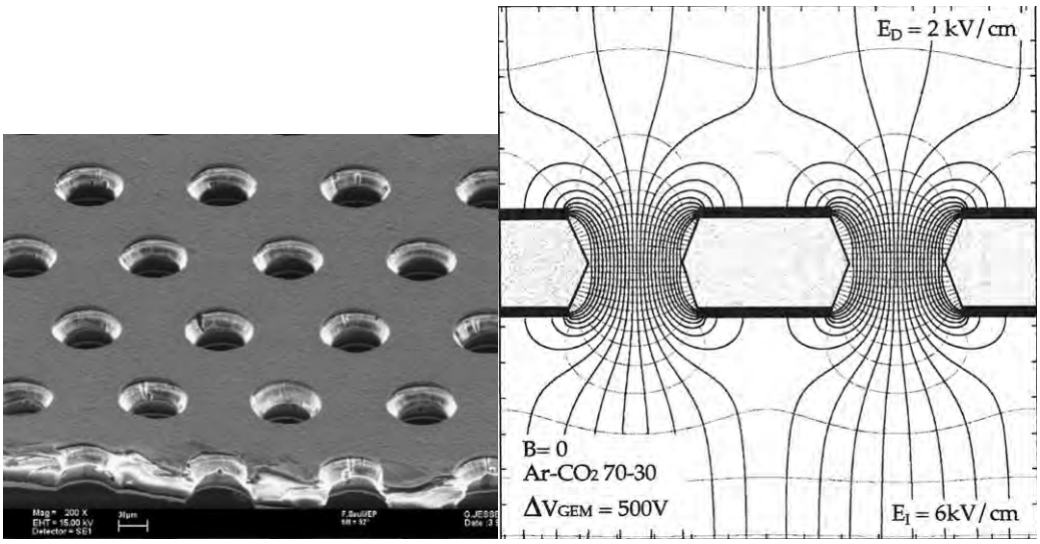

(a) The surface of th GEM foils (b) The electric field in holes

Figure 2.12: The photograph of GEM and the view of electric field[21]

The parameters of GEM foils in the E16 experiment are summarized below,

Table 2.3: The parameters of GEM foils

size(mm)	t1(μm)	t2(μm)	d1(μm)	d2(μm)	pitch(μm)
100	4	50	65 $\pm$ 5	35 $\pm$ 5	140
200	4	50	65 $\pm$ 5	35 $\pm$ 5	140
300 (12-div)	4	50	65 $\pm$ 5	25^{+10}_{-5}	140
300 (24-div)	4	50	55 $\pm$ 5	25^{+10}_{-5}	140

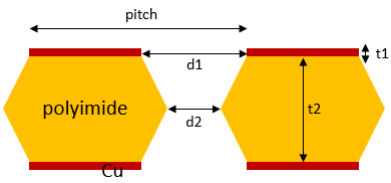

Figure 2.13: The parameters of GEM[20]

2.5.2 Readout

There are two dimensional strip readout, called "X" and "Y" strips. Both of them are perpendicular and the X-strips are correlated to the bending direction. For getting the high position resolution, the pitch of X strips is narrower than that of Y strips. Two types of readout board are used for three layers of GTR. For GTR100 and GTR200, they use the Blind Via Hole (BVH) type. The X strips are on the top side and the Y strips are on the bottom side. They are totally separated by polyimide (PI). The charge can transport between these two strips by the island electrodes which are also on the top side and connected to Y strips. For GTR300, the X and Y strips can be seen in the same side due to the PI is removed from the above of Y strips. This is called the PI-removed type.

Table 2.4: The pitch and width for each GTR[20]

	GTR100	GTR200	GTR300
type	BVH	BVH	PI-removed
pitch of x (μm)	350	350	350
width of x (μm)	125	125	70
pitch of y (μm)	1400	1400	1400
width of y (μm)	200	200	290

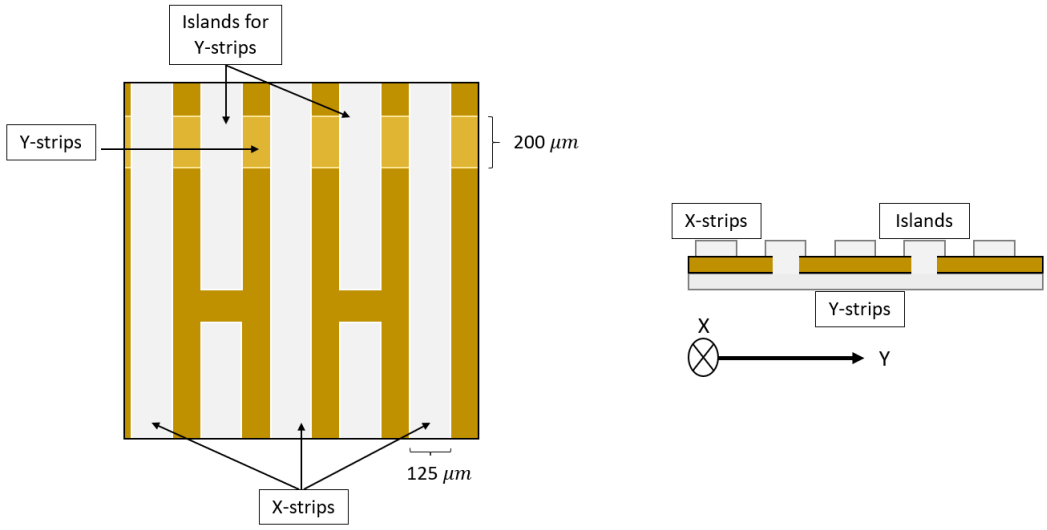

Figure 2.14: The schematic view of readout board for GTR100 and 200. The dark yellow plane is the PI, which is used to separate two directional strips.

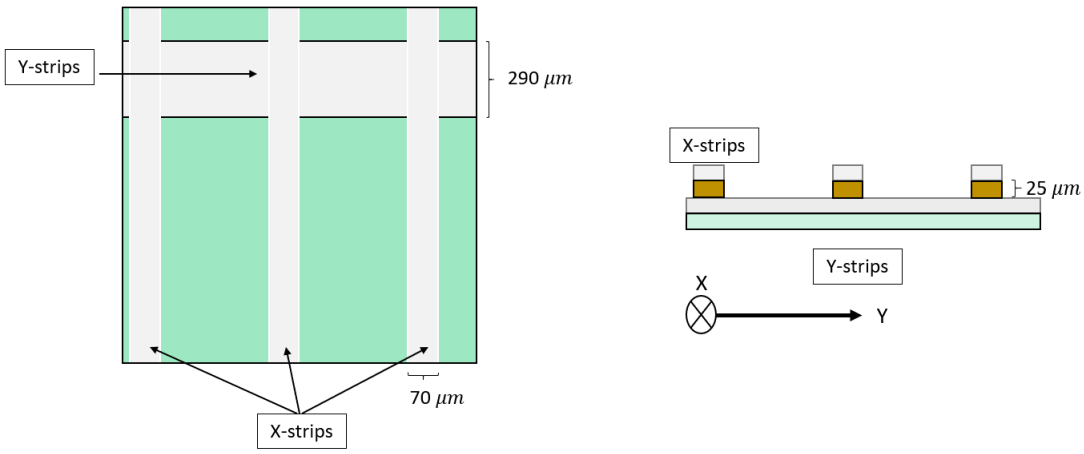

Figure 2.15: The schematic view of readout board for GTR300. The size of PI is the same as x-strips, which avoid two directional strips touch. The material of green color in the bottom is glass epoxy.

Chapter 3

Tracking performance and calibration

Track is reconstructed by one layer of SSD and three layers of GTR. After tracks of charged particles are established, position resolution and efficiency can be evaluated.

The reconstruction is divided into two part, one is track finding and the other is track fitting. Track finding starts from hit. Hit candidates are selected by electronic signal which satisfy the conditions and threshold we require. Then, several hits could be collected as a cluster, which is actually used for forming a track. The cluster are searched independently for X and Y strips on GTRs, but the requirement of pulse and timing information need to the same. Because there are three targets used in the experiment, track fitting are performed in two steps. The first fitting is to select a target out of three based on the best chi square. Next, the target position and hits position of four tracking detectors are used to reconstruct a complete track trajectory by a Runge-Kutta fitting. The projected points of HBD and LG are also determined in this step.

The position resolution is used as the weight of hit positions in tracking. If the values are too large, there will be a lot of fake fits included and thus fake track forms. The signal-to-background ratio in the mass spectrum will deteriorate. On the contrary, if the setting is too tight, it will reduce the efficiency of reconstructing the true events. However, before working on position resolution and efficiency, a calibration work is necessary and crucial. The position resolution of GTR was good enough in the previous studies[22] but it hasn't achieved to the goal of 100 μm. The new calibration will determine new parameters and check whether there are any correlation or bias. It is expected to obtain a better resolution after the calibration is done.

3.1 Calculation of hit position for GEM tracker

The hit position which used for the tracking is determined by the following instructions. It is determined at on the detector plane, which is assumed in the center of drift region. The concept about the hit position is shown in Fig. 3.1. The equation of hit position is shown as follows,

$$x = x_0 + lconst - z(\tan(\theta_{tr}) - \tan(\theta_l))$$

the z can be replaced by the drift velocity and time difference, so the equation will rewrite as,

$$x = x_0 + lconst - V_d \cos(\theta_l)(tdc - t_0)(\tan(\theta_{tr}) - \tan(\theta_l))$$

The meaning of each variables are as follows,
x: position at detector plane, which is used for tracking
x_0: measured position(hit strip)
$lconst$: x direction shift during detector plane to readout board due to Lorentz angle
z: distance between the cluster and detector plane
θ_{tr}: track angle
θ_l: Lorentz angle, between the electric field and the ionized electron drift direction
V_d : drift velocity, the direction is defined as moving of ionized electrons
tdc : tdc value for each hit candidate
t_0 : tdc value which corresponding to detector plane

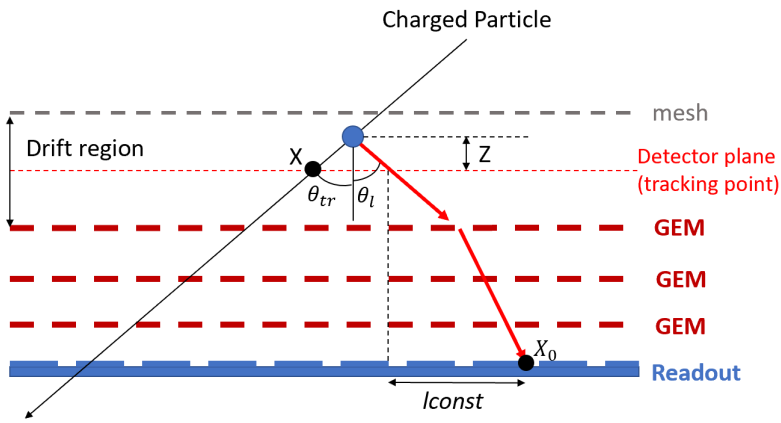

Figure 3.1: The concept of hit position.

In these variables, x_0 and tdc are measurement values, which come from the stored data in the experiment. θ_{tr} is a parameter decided track by track. The angle of track is determined by arctangent of distance of x and z. Finally, V_d, t_0, $lconst$ and θ_l are parameters to calibrate in the equation.

3.2 The items of calibration

There are five items for the GTR calibration, geometry, drift velocity (V_d), time (t_0), lorentz angle (θ_l) and offset constant ($lconst$). For geometry calibration, it was performed by "zero $\vec{B}$ field" run and then implemented as a file in all analysis. The result of geometry calibration showed that the correlation between residual and local position of GTR didn't have dependence in the middle part, but at the edge of the chamber, the calibration was not enough. It may be due to the distortion of the electric field and a lack of understanding of the drift behavior. At that time, the resolution had achieved to roughly 300 μm, it was good enough for track reconstruction. Therefore, currently we consider the other four items to have a further improvement. They are introduced in the following subsection.

3.2.1 Drift velocity and timing

In definition, drift velocity (V_d) is Proportional to electric field $\vec{E}$, which is controlled by applied voltage. At original analysis, V_d and time (t_0) was a constant parameter and had the same value in three layers of GTR and every module. However, it seemed that this simple assumption of a constant value is too naive for the reality situation of GTR detectors. First, the voltage of each layer was different. Then, the electric field was disturbed due to the charging up of the mylar. Furthermore, the structure irregularity of GEM or mesh also changed V_d. Table. 3.1 compares the setting of V_d and t_0 before and after the calibration in module 106[23]. In GTR100 and 200, the behavior of chamber is stabilized so that V_d and t_0 are a constant. However, in GTR300, the distance between mesh and first GEM is not uniform, some of positions have small distance, which cause a high V_d. So the V_d of GTR300 is set with a local position dependency. This change also affect the t_0, therefore, it is modified according to the V_d. These updated result is applied in the analysis.

Table 3.1: Comparison of the drift velocity and timing setting for different GTR layers in module 106

	layer of GTR	drift velocity(mm/ns)	time(ns)
Original setting	100/200/300	0.008	328
updated setting	100	0.013	265
	200	0.013	285
	300	$0.02\exp[-0.5(((x+130)/48)^2+(y/55)^2)]+0.012$	$1.5/V_d+180$

3.2.2 Lorentz angle and offset constant

In general, there is a strong $\vec{B}$ field applied in the experiment, so the drift property of ionized electrons would be modified. The Lorentz angle term is needed to take into consideration. In the simplest case, where $\vec{E}$ and $\vec{B}$ fields are perpendicular, the Lorentz angle can be achieved at[24]

$$\tan\theta_l = V_d \cdot \frac{B}{E}$$

but in reality, the relationship between $\vec{E}$ and $\vec{B}$ fields are more complicated. In the experiment, the electric field is not well understood in the part of Lorentz angle, so it is not easy to do the calibration from these variable. Therefore, the calibration work

of Lorentz angle is based on the original setting, where updated V_d and t_0 are applied iteratively until all results converge.

Lorentz angle and offset constant have individual value in each layer of GTR, but the same in each module. Like drift velocity, the value for every chamber is required. The calibration in this work is specifically for module 106. Currently, these two parameters are studied by the comparison between two data sets, run30322 and run30464, both of them are in run0c. The main difference is the direction of magnetic field, which is opposite. The advantage of using 30322 is that the GTR configuration is fine (drift voltage = 1800 V in GTR100/200, drift voltage = 1200 V in GTR300) and the trigger is single track since the multi-track trigger did not seem to work well in commissioning runs. The information of these two runs are shown in Table. 3.2. The reason for calibrating is that the timing dependence of residual on x direction is found and the mean of residual is shifted from zero with the original parameters. To check the phenomenon clearly and determine new value later, calibration using positive and negative charged tracks in run30322 and run30464 are studies separately. For convenience, they are called 30322pos, 30464pos and 30464neg in the later section. Because of the opposite magnetic field, actually the charged of 30464neg is the same as 30322pos, both of them are investigated for positive charged tracks. The negative charged tracks of run30322 are excluded since they don't have enough statistic. The procedure of analysis is described in Section 3.3.

Table 3.2: Information of run30322 and run30464

run number	purpose	trigger	intensity[/spill]	magnetic field
30322	e ID study	single track	4.4E+09	normal
30464	magnetic field scan	multiple track	8.3E+08	inverse

3.3 Calibration procedure for Lorentz angle and offset constant

To avoid the bias from the corresponding layer, the calibration is worked by the track fitting without hits of this layer. It is realized by setting an arbitrarily small weight for the hits on this specific layer so that the track is rebuilt by other three detectors. Because of an the opposite magnetic field, the sign of parameters for run30464 should be inverse. After selecting the tracks from several cut condition, the two-dimensional histogram of tdc value and residual for three cases (30322pos, 30464pos, 30464neg) is constructed, e.g. Fig. 3.2. On the left hand side, the figure is shown the tdc versus residual. It can help to check the distribution on these two variables. If all data points are projected on the direction of residual, the distribution is like the picture on right hand side. In order to check the correlation between tdc and the residual, the 2D histogram next is divided into several equal parts along the tdc direction. Then, distribution of residual in each timing slice could be gotten as Fig. 3.3. For obtaining the mean and sigma precisely, fitting is applied to each residual distribution. Generally, the fitting function uses a Gaussian together with a second order polynomial function to make sure the signal can separate from background. In some tdc slice, the statistic is limited so the function is a Gaussian with constant or Gaussian only. For each figure, in the statistic box, p0 to p5 are parameters for fitting function. The most two important terms are p1 and p2, which are center and sigma of gaussian respectively. They are used in the correlation graph. Fig. 3.4 is the correlation graph of tdc and the mean of residual. Tdc value is selected by the average of each timing area. The first and last point are chosen around the timing cut. The mean of residual is gotten from the fitting parameter p1. The points are drawn with a error bar to check the fitting result is reasonable.

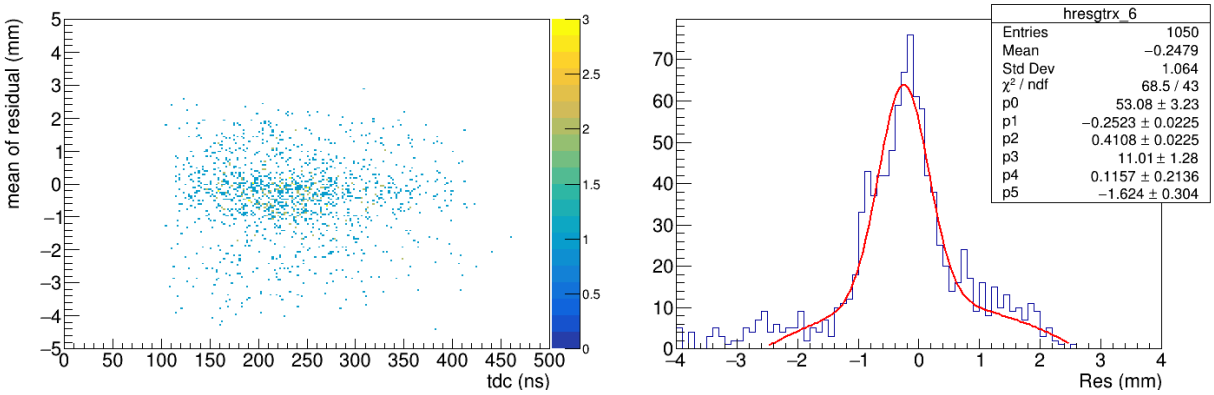

Figure 3.2: The histograms of tdc versus residual and total residual distribution for GTR100 in 30322pos

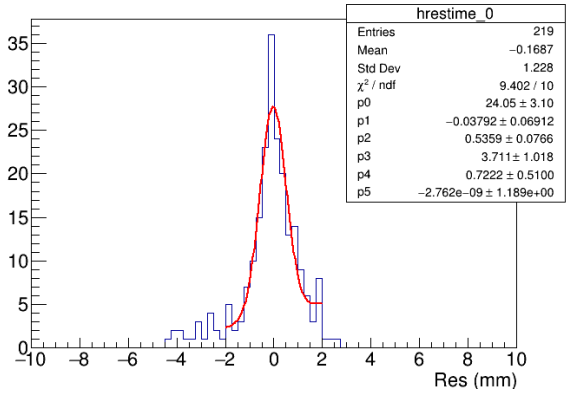

(a) $tdc < 180$

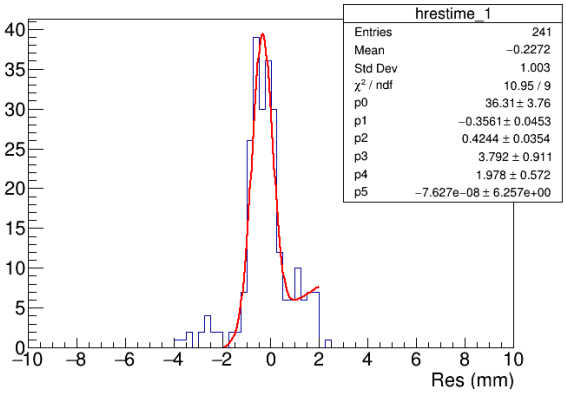

(b) $180 \leq tdc < 220$

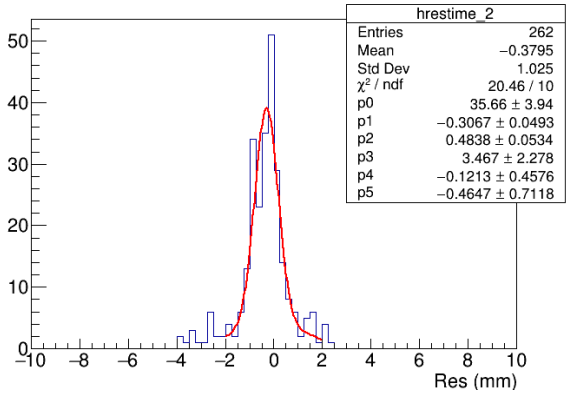

(c) $220 \leq tdc < 260$

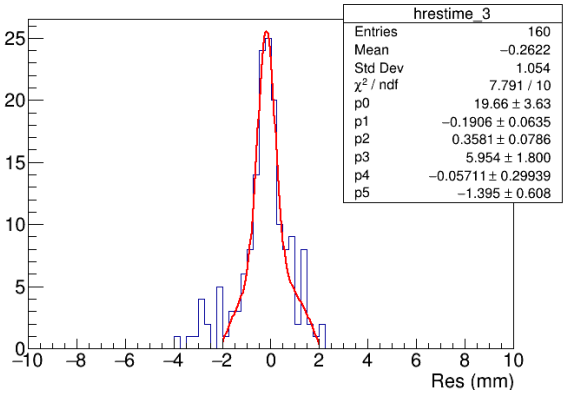

(d) $260 \leq tdc < 300$

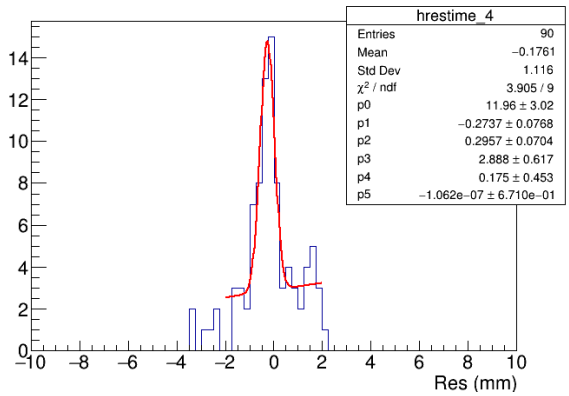

(e) $300 \leq tdc < 340$

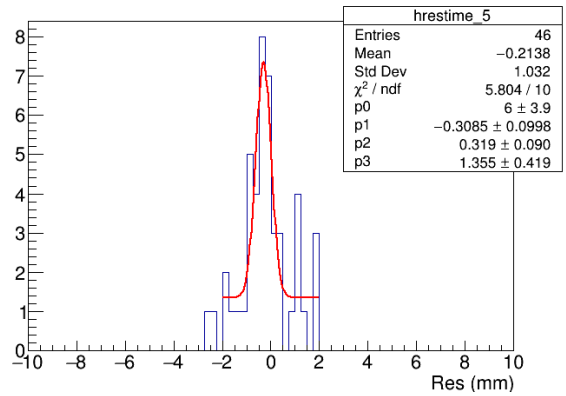

(f) $340 \leq tdc < 380$

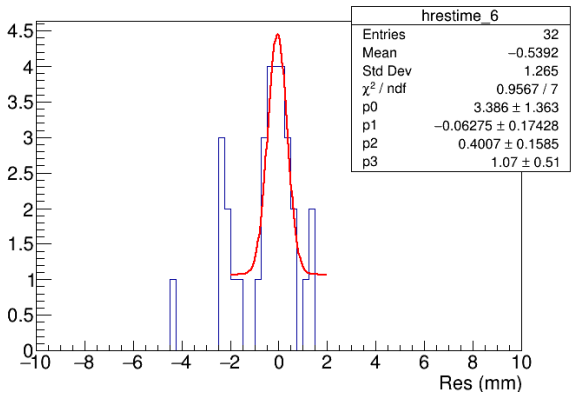

(g) $tdc \geq 380$

Figure 3.3: The residual distribution with fitting result in different tdc range for GTR100 in 30322pos

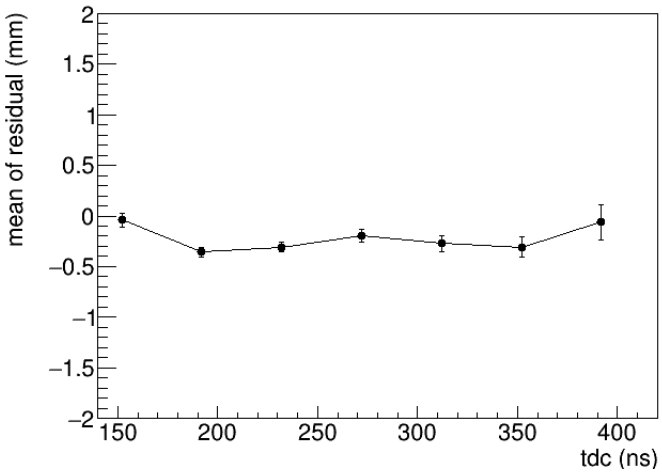

Figure 3.4: The correlation between tdc and mean of residual for GTR100 in 30322pos

The goal of study is to reduce the timing dependence on the residual and make the mean of residual close to zero. Thus, scanning of different parameter values in each layer of GTR is necessary. Different parameter combinations yield different correlation result. To do the quantitative research, each graph is fitted by the linear equation (y=ax+b) to check the severity of deviation by the slope and the constant. Fig. 3.5 is an example. In each parameter setting, the fitting is done for three cases (30322pos, 30464pos, 30464neg) simultaneously and then taking an average value to compare which parameter setting is suitable.

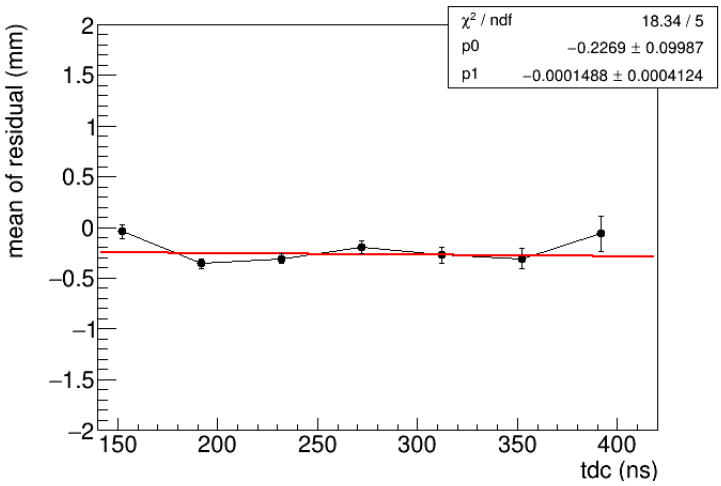

Figure 3.5: The correlation between tdc and mean of residual with linear fitting for GTR100 in 30322pos

The calibration starts from the Lorentz angle term, which is related to the timing dependency of residual. The slope of linear equation has a significant change when Lorentz angle is altered. It can be checked from the Fig3.6. These three figures bring up two important points. (1) Due to an opposite magnetic field, the direction of correlation graphs of run30322 and run30464 are inverse. (2) All of color lines in each figure are overlapped with a value, which is a setting of tdc for corresponding to detector plane in the equation.

The goal of Lorentz angle setting is to minimize the slopes in three cases. Therefore, the selection criteria is defined as,

$$slope_{min} = \sqrt{(slope_{30322pos})^2 + (slope_{30464pos})^2 + (slope_{30464neg})^2}$$

The weight of three cases are the same, and in this moment, the mean of the residual is not considered because it will be tuned later in the offset constant.

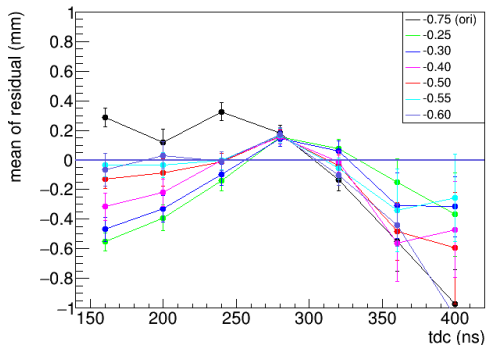

(a) run30322 positive charged track

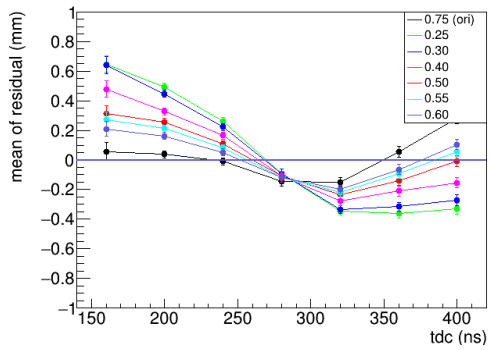

(b) run30464 positive charged track

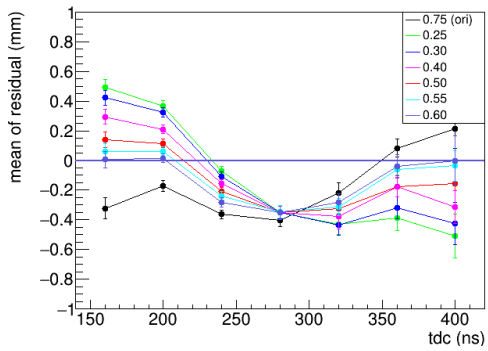

(c) run30464 negative charged track

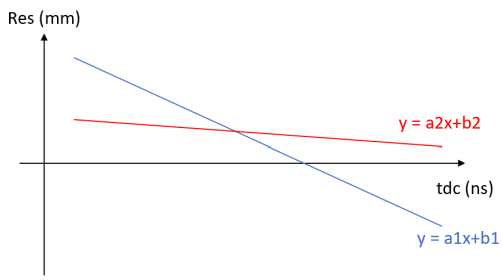

(d) The schematic view of fitting result for two different Lorentz angle

Figure 3.6: The correlation between tdc and mean of residual with different Lorentz angle for GTR200 in three cases

After finishing the work of Lorentz angle, the updated parameters are used in the analysis and then continue to tune the offset constant. For offset constant, the mean of residual in each timing area is shifted when the value is changed, so it is corresponding to the constant term in the linear equation. The behavior can be seen in Fig. 3.7. With a large change in offset constant, there is a significant displacement. In this step, we would like to find a value where the mean of residual is close to zero as much as possible. It means that the constant term in fitting function should be small. In order to make three cases satisfy the requirement simultaneously, the average value is performed to decide the parameter. Here, not only the timing dependency of residual is used for selecting the offset constant, local x and local y dependence needs to be taken into account. Local x and y mean that the position is defined at each detector rather than whole spectrometer. The correlation between local x/y and mean of residual can be obtained in a similar way as the tdc dependency. So, the final selection criteria becomes as,

$$cont_{min} = \sqrt{const_x + const_y + const_t}$$

where,

$$const_x = (x_{30322pos})^2 + (x_{30464pos})^2 + (x_{30464neg})^2$$
$$const_y = (y_{30322pos})^2 + (y_{30464pos})^2 + (y_{30464neg})^2$$
$$const_t = (t_{30322pos})^2 + (t_{30464pos})^2 + (t_{30464neg})^2$$

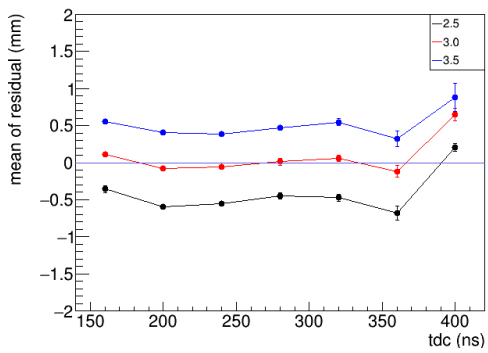

(a) run30322 positive charged track

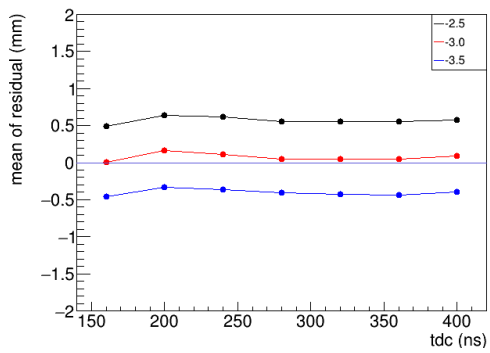

(b) run30464 positive charged track

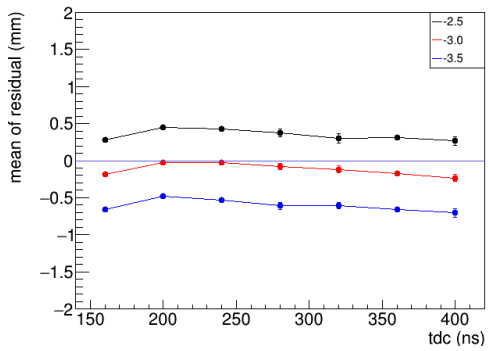

(c) run30464 negative charged track

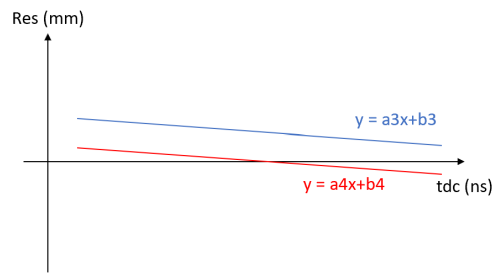

(d) The schematic view of fitting result for two different offset constant

Figure 3.7: The correlation between tdc and mean of residual with offset constant changed for GTR100 in three cases

If Lorentz angle (offset constant) in three layers of GTR are independent, they can be tuned individually and then combined the results each other in the final step. However, due to the correlation of hits on different layers in tracker, the method to find new parameters is to loop through three layers of GTR several times. The flow chart of method is shown in Fig. 3.8, where a calibration of Lorentz angle (θ_l) is taken as an example. The parameters of three GTRs are set as a array $\theta_L = \{\theta_{l1}^x, \theta_{l2}^x, \theta_{l3}^x\}$. For each element, the number in subscript shows the corresponding layer of GTR and the superscript is for recording the round of calibration. It starts from 0 to n, according to how many times of calibration is preformed, so the original setting can be written as $\theta_L = \{\theta_{l1}^0, \theta_{l2}^0, \theta_{l3}^0\}$. The demonstration in the following is started from original setting of GTR100. The value of θ_{l1}^0 is altered to different value while the other two remain as original one. The difference of correlation and the determination of minimum slope have been introduced before. The parameter corresponding to the minimum slope is selected from them, called θ_l^{tmp}. This value would not be used in the next layer calibration in order to decrease the effect of dependence between each layer. The new value is a arithmetic mean from original and θ_l^{tmp}. Then it replaces the original value of GTR100. Because the first time calibration is finished, the superscript of θ_{l1} will plus one. This result of θ_L is applied in next layer. For GTR200, with the similar process, new parameter for GTR200 is obtained and now two elements of θ_L are altered. Then, it is turned to the work for GTR300. After three layers of GTR are completed the first time of calibration, the parameter array becomes $\theta_L = \{\theta_{l1}^1, \theta_{l2}^1, \theta_{l3}^1\}$, which means first round is finished and it can continue to next round. In each round, the common difference and the scanned range gradually become smaller and the value finally converges. The $\theta_L = \{\theta_{l1}^n, \theta_{l2}^n, \theta_{l3}^n\}$ is the final parameter setting for each GTR.

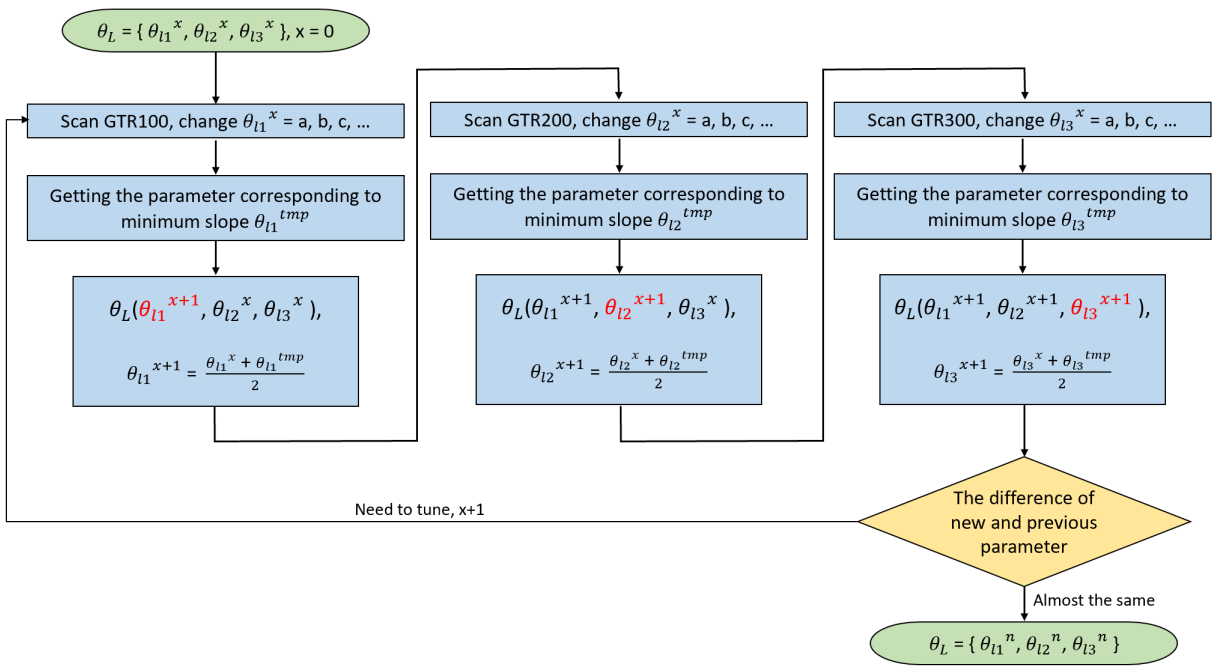

Figure 3.8: The flow chat of finding new parameters for Lorentz angle

3.4 Result of calibration

3.4.1 Comparison of correlation graphs in three data

After determining the new parameter setting of Lorentz angle and offset constant, the final correlation graphs for three layers of GTR are shown in Fig3.9 ∼ Fig3.11. The mean of residual is correlated to (a) local position x, (b) local position y and (c) tdc. Each figure has three cases, black solid circle is for 30322pos, blue solid square is for 30464pos and red solid inverted triangle is for 30464neg. The residual distribution and fitting result of each point offer in the Appendix B. The observation and conclusion related to the points for these figures are discussed below.

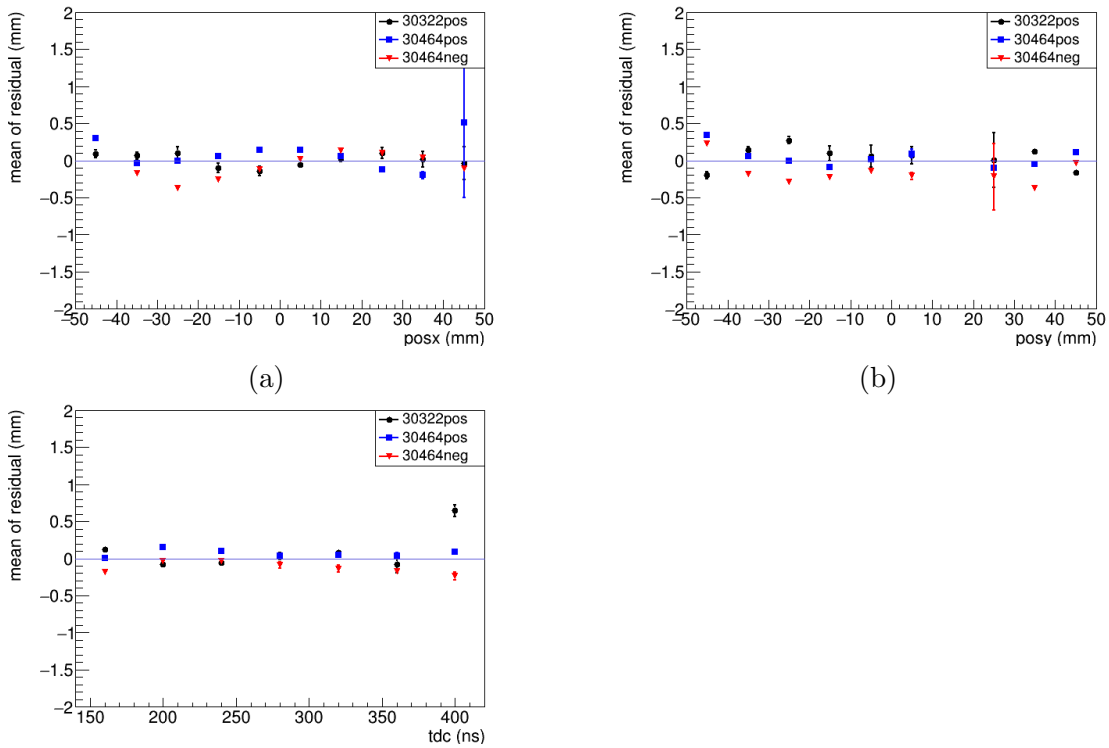

(a) (b) (c)

Figure 3.9: The correlation between (a)posx/(b)posy/(c)tdc and mean of residual with final parameter setting in GTR100 for three cases

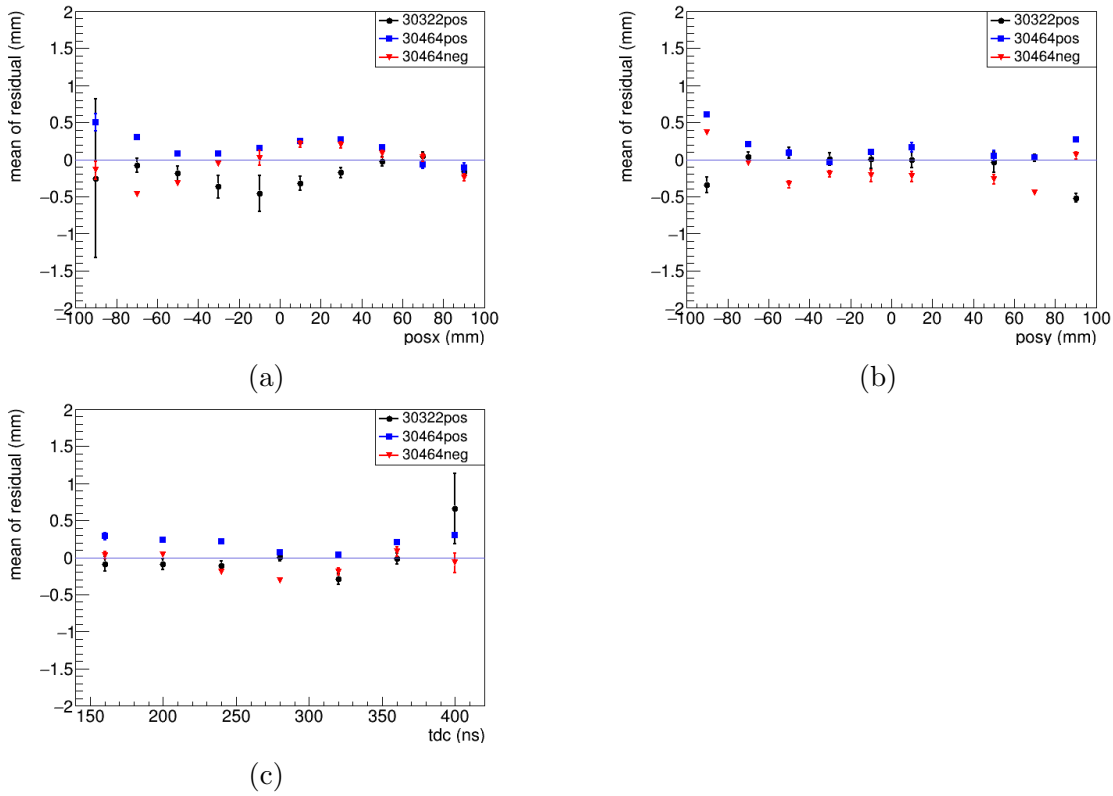

Figure 3.10: The correlation between (a)posx/(b)posy/(c)tdc and mean of residual with final parameter setting in GTR200 for three cases

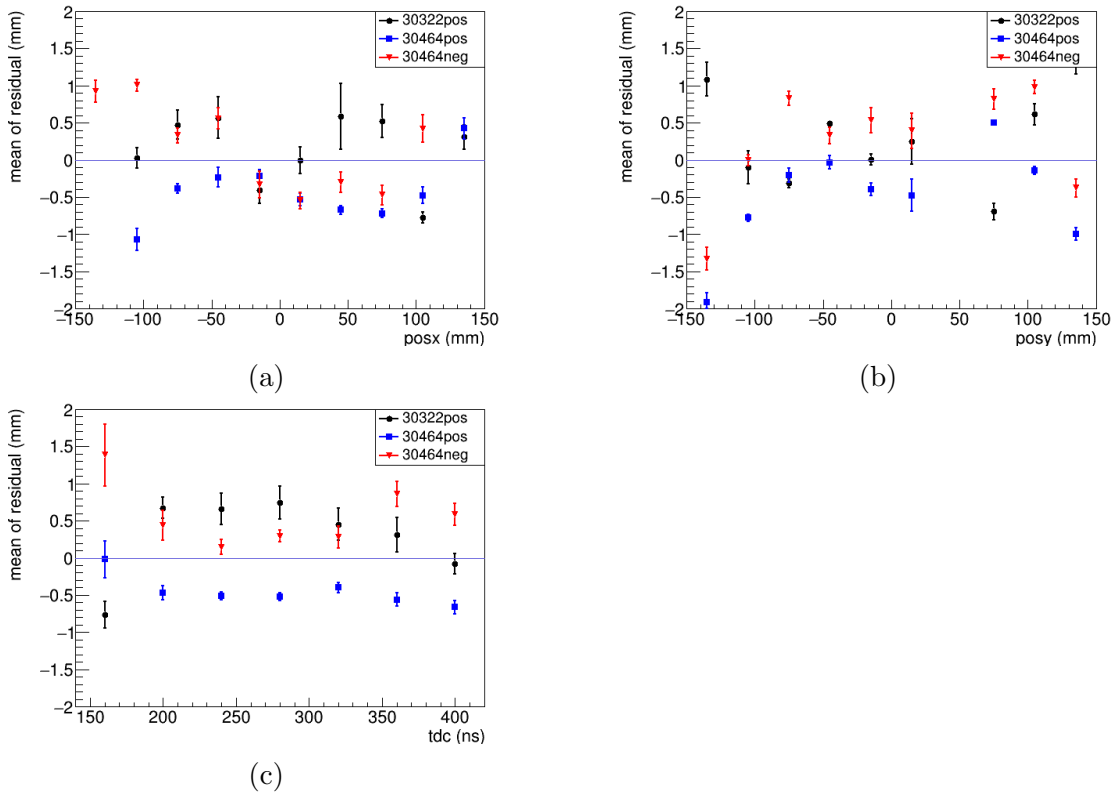

Figure 3.11: The correlation between (a)posx/(b)posy/(c)tdc and mean of residual with final parameter setting in GTR300 for three cases

(1) Dependency
From these results, because the parameters are decided from three cases with the same weight, it is hard to satisfy them close to zero simultaneously. If the correlation of one of case is required to be zero, the others will have a great shift. Even in the same run (30464), positive and negative charged tracks have different behavior. The residual distributions as a function of position x, position y and tdc in three cases show the best consistency in GTR100 among the three layers, especially for timing dependency. GTR200 is also not bad, and the effect of inverse magnetic field can be observed, as that the curve in Fig. 3.10(a) and (b) for 30322 and 30464 are opposite. However, in GTR300, the deviation appears clearly and it seems that dependence still exists. For the correlation of time, although the dependency has been reduced, none of them are close to zero. On the other hand, the correlation of local position X and Y also do not match each other and the mean positions are very different in each area. There may be some other factor or issue must to consider. To illustrate the improvement with the new parameters, a comparison of the residual distributions with the old and new calibration parameters will be shown in the Section 3.4.2.

(2) Fitting issue
In order to perform the fitting efficiently, the simplest and most efficient method is usage of the same fitting function and identical condition. However, there are three problems found during the calibration work so that some of them are needed to modify.

1. In some area, the statistic is not well enough. It is even zero in the local position of Y direction. The situation is caused by the effective area of detector and geometry during that experiment run, where some of strip may be dead.

2. The signal-to-background ratio is different for residual distributions. Usually they can be checked a significant peak in Gaussian shape. However, some of them, the signal is hard to distinguish from background.

3. The width of distributions from narrow to broad are GTR100, GTR200 then GTR300. This reason is because GTR300 is the last detector for track fitting and the investigation of dependency is needed to exclude the corresponding detector. Without next hit position to constrain the track, the deviation on GTR300 will be larger than others.

3.4.2 Comparison of different parameter setting

Table. 3.3 shows the parameter setting before and after calibration for each layer of GTR. There are positive and negative values for different layer of GTR. The reason is that the GTR100 is placed upside down in terms of its local coordinate so the values should be opposite between GTR100 and GTR200/300 in the analysis.

Table 3.3: Parameter setting before and after calibration

	layer of GTR	Lorentz angle(rad)	offset constant(mm)
Before calibration	100	0.313	2.625
	200	-0.233	-1.925
	300	-0.129	-1.05
After calibration	100	0.219	3.023
	200	-0.617	-2.408
	300	-0.135	-1.095

Comparing these values, most of parameters only have a slight change, but the Lorentz angle in GTR200 become significantly large. We do not have a good understanding of this observation. In order to check the improvement of residual dependency using the updated parameter, the following figures show the results of three different conditions in module 106, for 30322pos. In Fig. 3.12 $\sim$ Fig. 3.14, we not only shown the correlation between posx/posy/tdc and mean of residual, but also posx/posy/tdc versus width of residual from study 1 to study 3 for each layer of GTR. For every points in the correlation graphs, the residual distribution and fitting result offer in the Appendix B.

- study 1 - The most original setting in the analysis, without any calibration on drift velocity, tdc, Lorentz angle and offset constant.
- study 2 - With only using updated drift velocity and tdc, the Lorentz angle and offset constant still remain as the original one.
- stidy 3 - With using updated drift velocity and tdc, the Lorentz angle and offset constant are also set as after calibration.

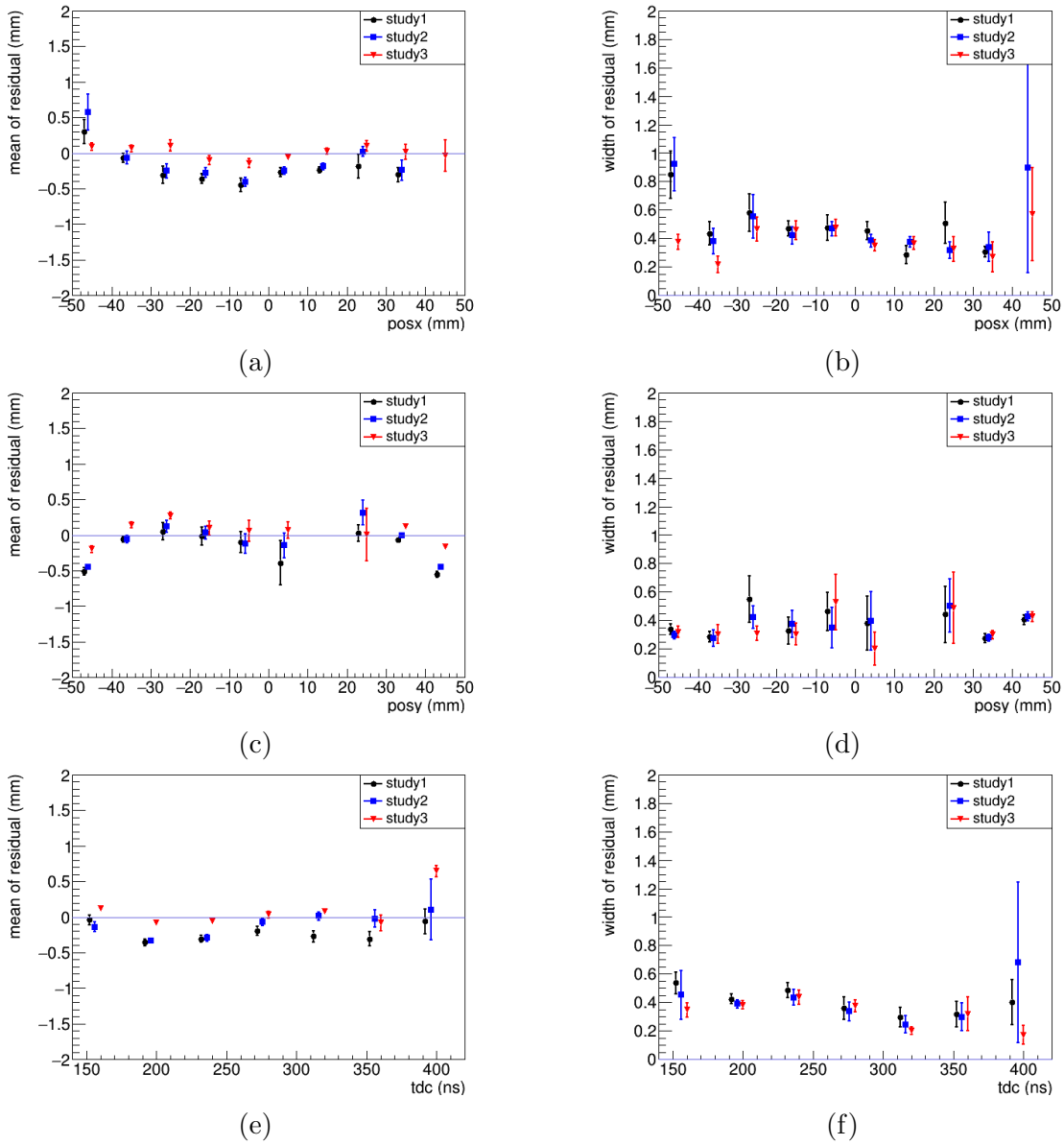

Figure 3.12: The correlation between posx/posy/tdc and mean(a)(c)(e)/width(b)(d)(f) of residual in GTR100 with three studies

For GTR100, the dependency is actually not strong, but it can still be found that the positive correlation in low timing area and a curve in the middle part of x position. If the parameters only affect the drift velocity and tdc, the distribution for study 1 and study 2 in position dependency are almost the same. In timing dependency, it shows an improvement and locates at zero in high timing area. After calibrating four kind of parameters, the dependencies in position and time are removed. In Fig. 3.12(c), correlating to position Y, the change is very insignificant but the bias on the edge is reduced compared with the original one. The last points for every study in Fig. 3.12(e) are unreliable because of a lack of statistic.

On the other hand, when we check the width of residual in different variables and every studies, they are almost consistency. All of them are 400 μm, but the final width still needs to check from the total residual distribution.

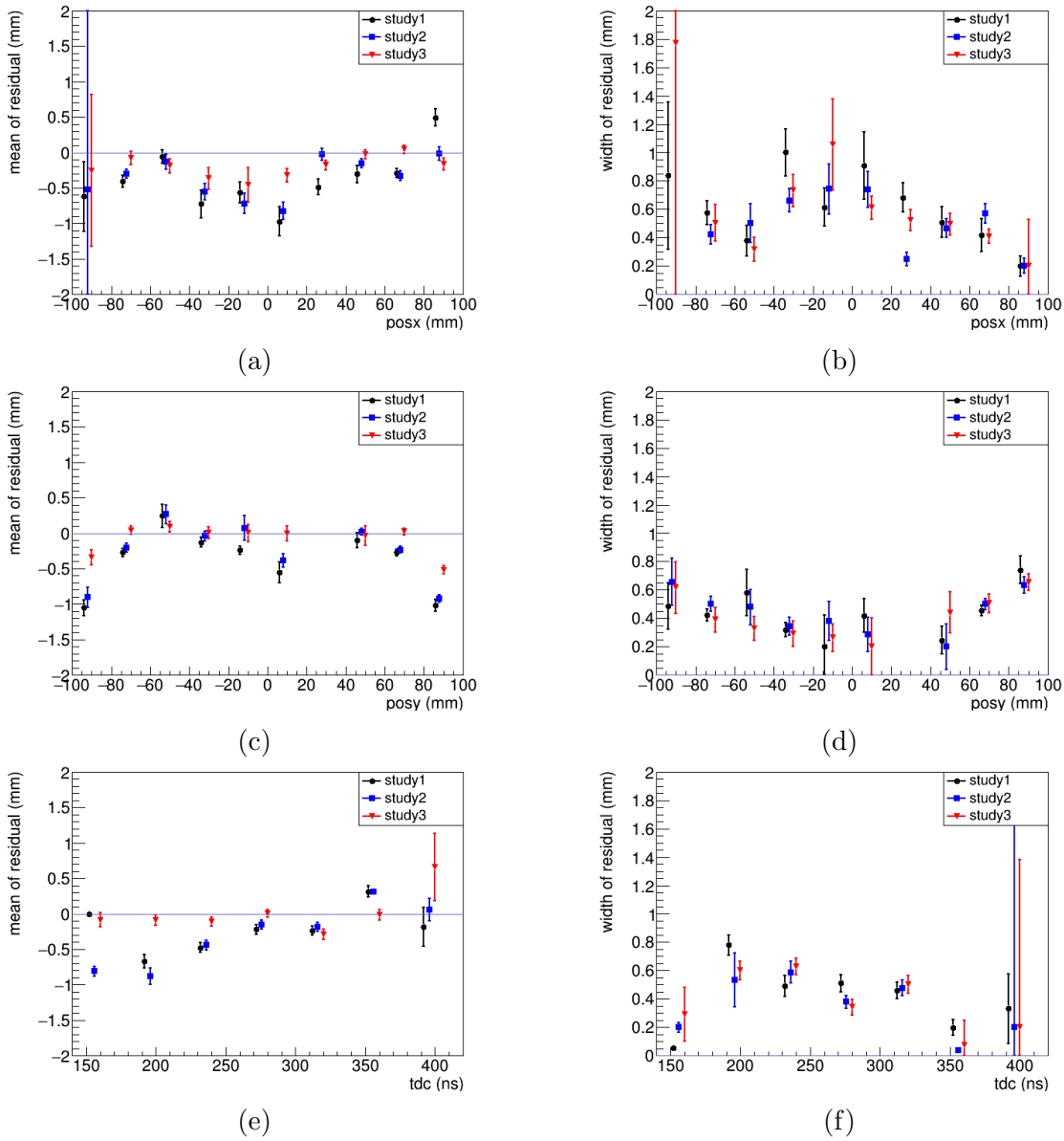

Figure 3.13: The correlation between posx/posy/tdc and mean(a)(c)(e)/width(b)(d)(f) of residual in GTR200 with three studies

For GTR200, the correlation plots of mean of residual in the study 1 show a strong dependence. In timing dependency, the slope is larger than which in GTR100. The gap of curve in position dependency also become bigger. In study 2, the change is not visible clearly. That shows a successful calibration. All points in study 3 for posy and tdc are very close to zero, only the result in posx has a tendency to the negative side. The fitting also fails in the first point in Fig. 3.13(a) and last point of in Fig. 3.13(e), due to small statistic.

In the correlation plots of width of residual, we find that the width becomes large in the middle part of position x but small in the middle part of position y. It seems that the width of residual is different in the position x and y direction. It is hard to check the variation of width in these three figures.

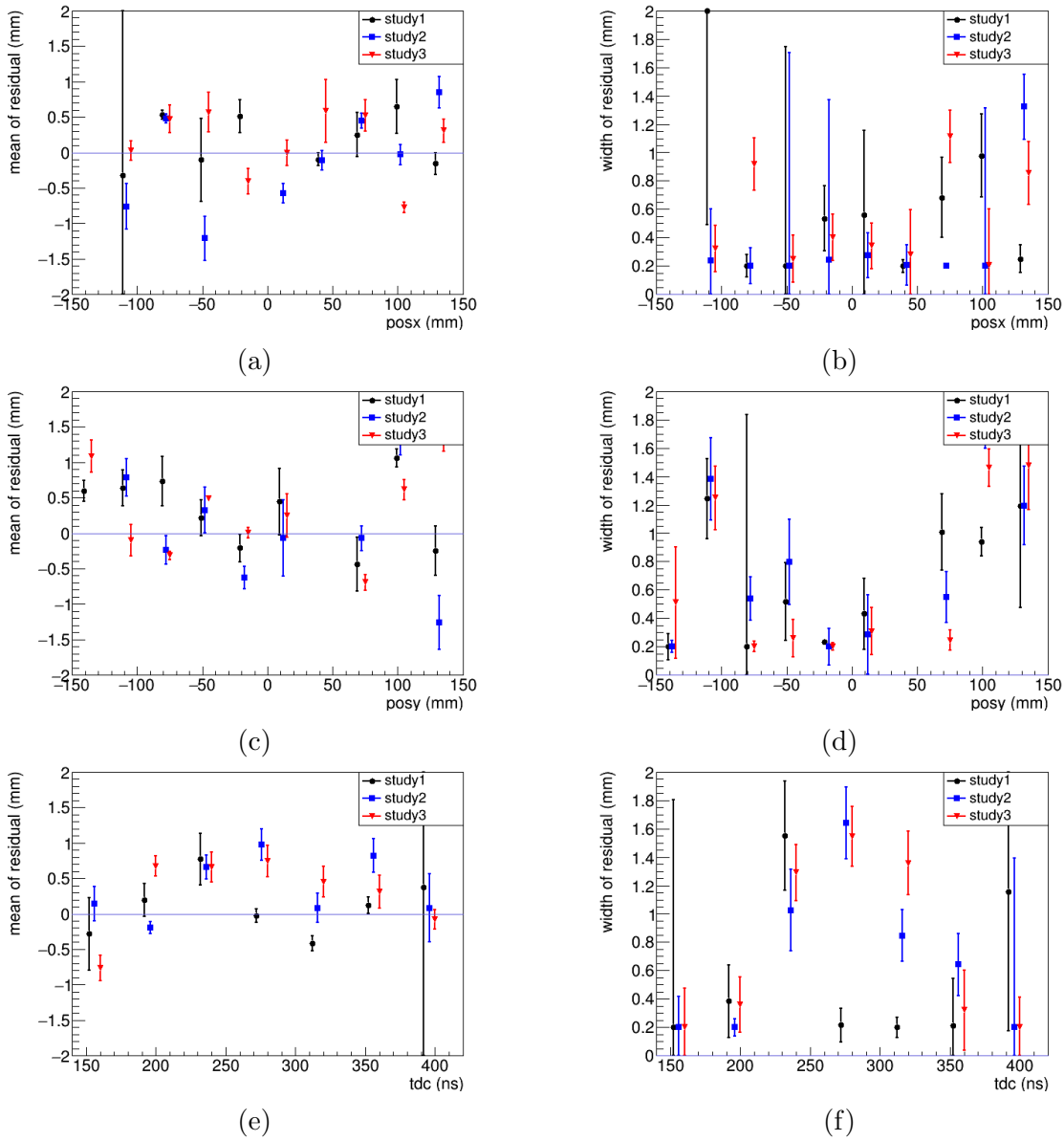

Figure 3.14: The correlation between posx/posy/tdc and mean(a)(c)(e)/width(b)(d)(f) of residual in GTR300 with three studies

For GTR300, it is difficult to make a conclusion for GTR300 currently because no clear correlation is found in any of the studies. Two adjacent point seem independent and error bars are larger than which in previous two layers of GTR. If we go back to check the every residual distribution with fitting. Most of distributions have a wide and flat background with a unclear signal. It is hard to see the Gaussian distribution in these plots, so no matter which fitting function, Gaussian, Gaussian with constant or Gaussian with second polynomial can not depict them well. Only the correlation of timing dependency for study 3 has a higher credibility, but it is shifted away from zero also. The GTR300 calibration may need to work again with a more accurate way.

One speculation for worse behavior of GTR300 is the low drift voltage setting in this run. But in order to resolve these problem currently, there are two possible methods to try. One is that includes more run data to increase the statistic for GTR300, but the effect of track fitting without GTR300 may still cause a worse result in each slice. The other method is to construct a mean of residual by the arithmetic mean rather than using

fitting function. However, background entries may also be contained, it will make a bias for real signal.

Finally, we show the total residual distribution of x direction for each layer of GTR before and after calibration in Fig. 3.15 because some the behavior can not clarify in the slices, such as the width of residual. The purpose is to check if the mean of residual is close to zero and the width of the signal becomes smaller with the new parameters. The sigma of residual fitting is one important component to evaluate the resolution in next chapter. Table. 3.4 shows the two critical information from Fig. 3.15. The parameter term "p1" is corresponding to "mean of residual" and "p2" is referred to the "width of residual" in figures. According to the table, the mean is closer to zero in new consequence, but the sigma for each layer is nearly unchanged except the GTR200, which has an approximately 100 μm reduction. The major effect of the calibration work seems to shift the residual distribution but only slightly reduce the width.

Table 3.4: Result of fitting before and after calibration

	layer of GTR	mean(mm)	width(mm)
Before calibration	100	-0.2523 ± 0.0225	0.4108 ± 0.0225
	200	-0.4584 ± 0.0414	0.6919 ± 0.0467
	300	0.9468 ± 0.1426	1.463 ± 0.138
After calibration	100	0.0027 ± 0.0189	0.4196 ± 0.0215
	200	-0.1511 ± 0.0332	0.5372 ± 0.0462
	300	0.3941 ± 0.0867	1.402 ± 0.094

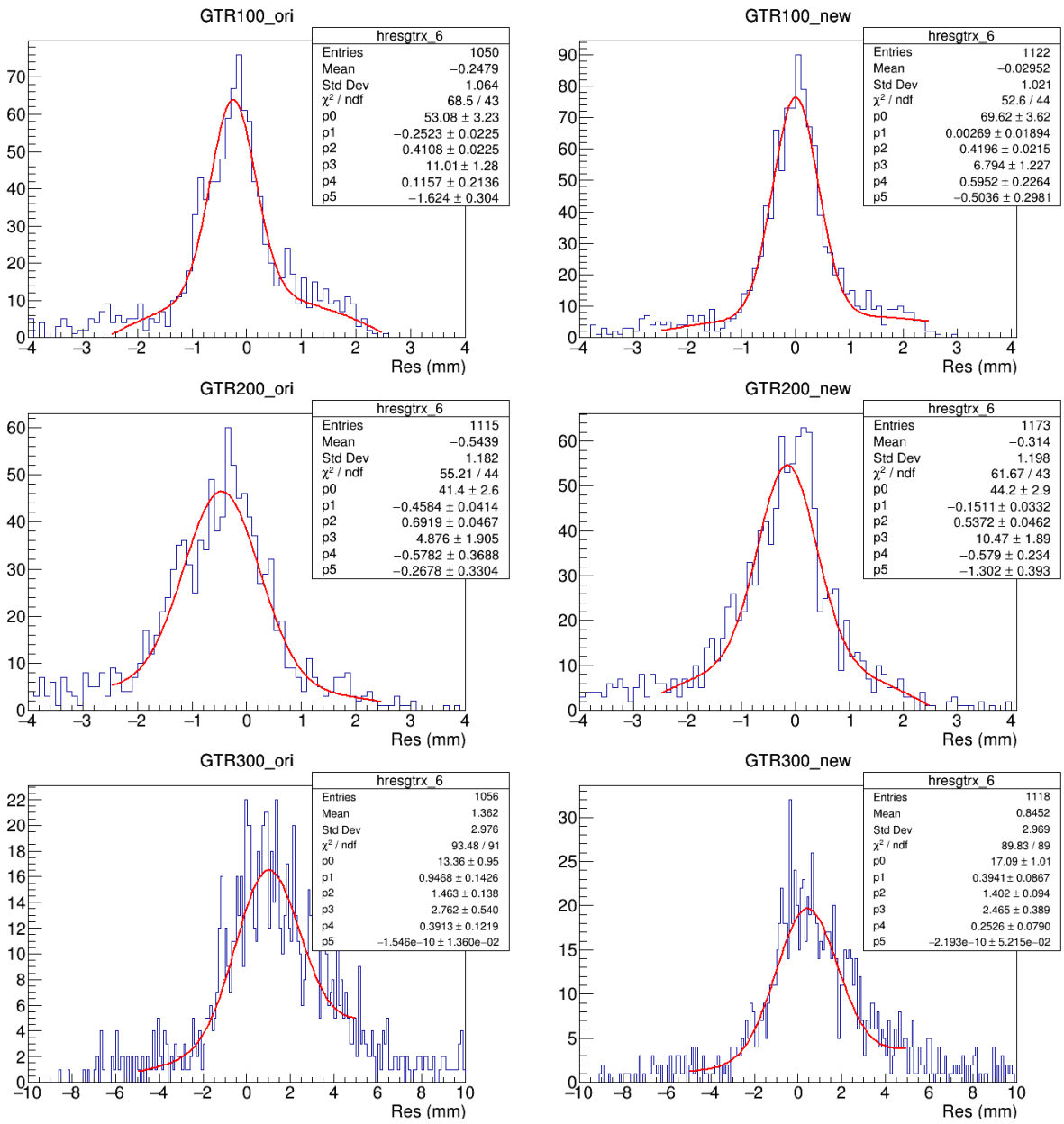

Figure 3.15: The residual distribution with fitting result for different parameter condition. The figures on left hand side are study 1(before calibration) and the figures on right hand side are study 3(after calibration)

Chapter 4

Position resolution and efficiency of GEM tracker

The purpose of the calibration work is to enhance the position resolution and then check the efficiency of three layers of GTR. Currently, in J-PARC E16 Technical Design Report[22], the position resolution of three layers of GTR are roughly 300 μm, which is a acceptable result for measuring mass modifications of vector mesons. In this chapter, the position resolutions and efficiencies with new parameters are evaluated. The calibration work is performed for one of module, module 106, with the run0c data 30322.

4.1 Position resolution

We introduce a method for evaluating the position resolution : the "geometric-mean method[26][27]". This is a popular method used to determine the position resolution of tracking detector such as GEM tracker. To begin with, the track fitting used Runge-Kutta is performed twice. First one, track is reconstructed with the inclusion of a relevant detector. In other words, hits of the relevant detector are used in the fitting. The other one is done by excluding hits of a relevant detector, so the fitting is performed only with the hits of the detectors. The schematic of including and excluding one detector are shown in Fig. 4.1, where GTR100 is taken as an example. Without the bias from GTR100, the projection position of detectors may be changed. Next, the analysis for picking "true" track candidates is worked. This part will be illustrated in next section. Thirdly, residual distributions of including and excluding relevant detector are obtained and the fitting result of distributions are acquired. Finally, the position resolution of a relevant detector can be approximated by the geometric mean

$$\sigma = \sqrt{\sigma_{in}\sigma_{ex}}$$

where σ_{in} is the standard deviation of residual distribution obtained from the fitting with all tracking layers, and σ_{ex} is the one corresponding to the track fit excluding the relevant detector. The advantage of geometric mean method is that the position resolution would not be overestimated by the detector bias and not get faulty result in removing one detector layer.

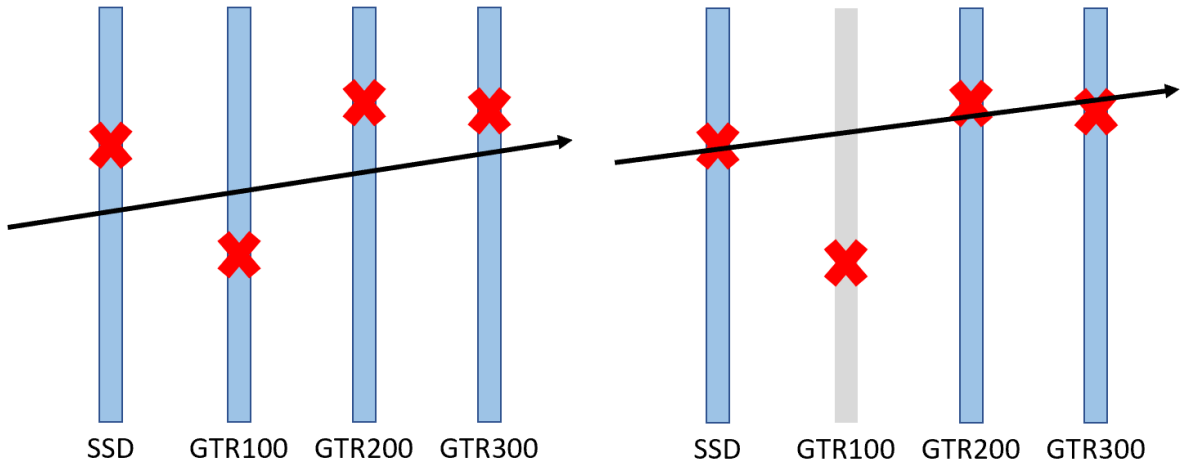

(a) GTR100 included (b) GTR100 excluded

Figure 4.1: The schematic of track fitting with and without hits of GTR100

4.2 Analysis of position resolution

The Runge-Kutta fitting selects all of possible combination to get a track, so there could be many fake tracks if background hits are many. To choose a true track for a residual distribution, some cuts to suppress the fake ones are applied. The first one is the high multiplicity events cut. If one event has too many track candidates, it is thrown away. Next, the track candidates which in the passed event are surveyed one by one. Fundamental cuts are the requirements on the chi square, charge, detector module and momentum of the track candidates. However, the applying of these cuts can not obtain the reliable residual distribution. Fig. 4.2 demonstrates the residual distribution with the fundamental cuts for GTR100 in x direction, for the case of track fitting excluding GTR100 itself. A lot of entries occupy around zero, it is hard to distinguish signal from background.

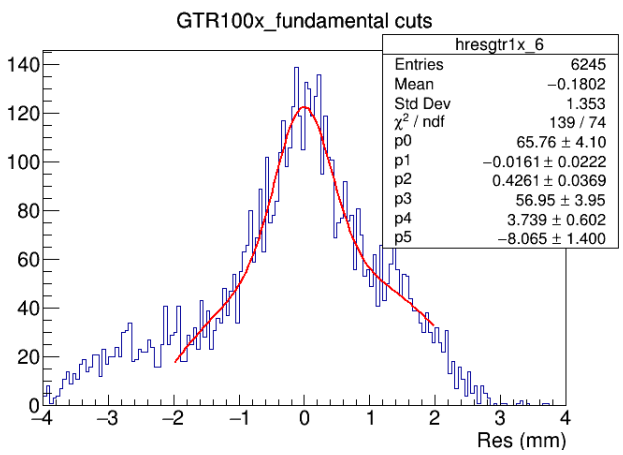

Figure 4.2: The residual distribution of GTR100x with fundamental cuts

Then, HBD association is required, this step is used to check whether a projection position has match hits of HBD. By the way, to avoid two or more track candidates associating the same HBD hit, a cut of duplicate hit is applied. With the above cut

conditions, a clear signal of residual distribution can be observed. Fig. 4.3 is the residual distribution of GTR100x with the HBD association. Compared to previous result in Fig. 4.2, lots of uncorrelated entries are removed by this cut.

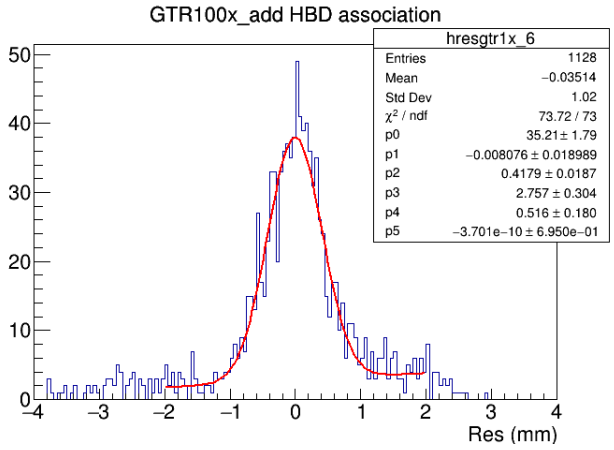

Figure 4.3: The residual distribution of GTR100x with using HBD association

LG association

The effect of LG association is similar to the HBD association. It is used to check whether a projection position has match hits on LG. Fig. 4.4 shows the residual distribution with LG association. Entries are much less than which only use HBD association, and the standard deviation is further reduced.

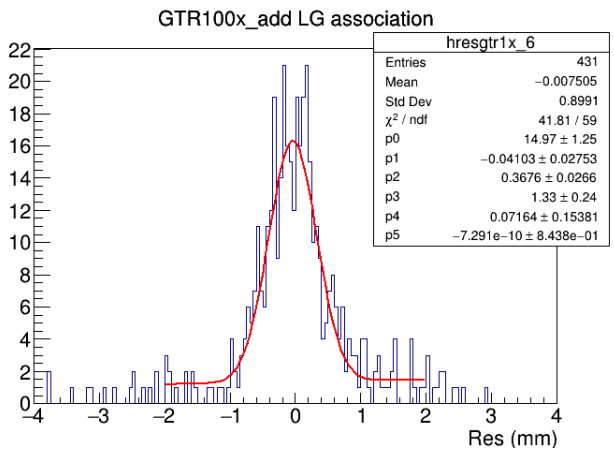

Figure 4.4: The residual distribution of GTR100x with using LG association

Tracks in the same module

Because the track could traverse two different modules in upstream and downstream GTRs. To make the situation clear, track candidate is required to pass module 106 only in three GTRs. Fig. 4.5 shows the residual distribution of tracks traversing the same module. Only a few entries are removed, so the result is almost the same as Fig. 4.3.

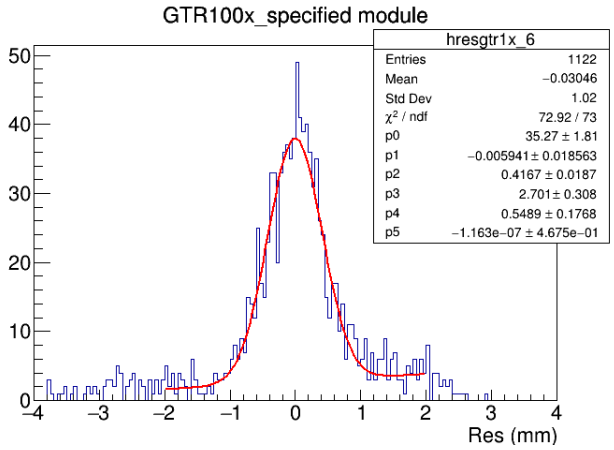

Figure 4.5: The residual distribution of GTR100x with confining to the same module

Cut from other GTRs' residual

To let a track has high correlation among all layers in x and y direction. The residual in other GTRs are used as the cut conditions. For example, if the analysis is for residual of GTR100X or Y, the residual of GTR200X and Y, GTR300X and Y are required. Here, the case of all layer fitting and excluded single layer need to discuss respectively.

For all layer fitting case, the residual distribution for a layer which use to evaluate the resolution has a strong correlation with others, especially in X direction. The phenomenon can be checked in the Table. 4.1. In the studies of GTR100 and GTR200, the removal of residual cuts on gtr2x or gtr1x plane yields similar residual values without any residual cuts on all other planes. Therefore the residual cut on the gtr2x (gtr1x) plane introduces the most significant systematic effect on the residual of GTR100 (GTR200). For unknown reason, there is no similar observation for the study of GTR300. As a result, for residual of GTR100X, the result is mainly influenced by GTR200X. For residual of GTR200X, the result is mainly influenced by GTR100X. And for residual of GTR300X, it seems that the result is influenced by GTR100X and GTR200X both.

Table 4.1: The standard deviation of residual for three GTRs in x direction with different GTR residual cut

	without cut	with all cut	wo gtr2x	wo gtr2y	wo gtr3x	wo gtr3y
GTR100	282	181	264	182	181	181
	without cut	with all cut	wo gtr1x	wo gtr1y	wo gtr3x	wo gtr3y
GTR200	220	143	205	144	143	142
	without cut	with all cut	wo gtr1x	wo gtr1y	wo gtr2x	wo gtr2y
GTR300	82	44	45	44	55	44

On the other hand, the different range of cuts are also checked. The cuts used in Table. 4.1 are tightest, so we loosen the cut on the main bias part to check if the residual could converge. The results is shown in Table. 4.2. It seems that the correlation is too strong to find a constant.

Table 4.2: The standard deviation of residual for three GTRs in x direction with different range of cut on bias layer

	gtr1x (±0.3 mm)	gtr1x (±0.6 mm)	gtr2x (±0.3 mm)	gtr2x (±0.6 mm)
GTR100	×	×	191	263
GTR200	127	187	×	×
GTR300	39	45	47	55

For excluded single layer, the width of residual distribution of corresponding analysis layer is become wider than the all layer fitting case, but residual in other GTRs are turned into very narrow. So no matter what kind of cut range in the all layer fitting case do not effect the residual distribution.

Cut of local position of Y direction

In chapter 3, the result of correlation between posy and mean of residual. It is found that there are bias on the edge. The residual behavior at the edge part cannot be well explained even with zero magnetic field as mentioned in Section 3.2. So, we are curious that if the edge is removed, the residual distribution will change or not. Fig. 4.6 to Fig. 4.11 show the local position Y versus residual X for three GTRs. The all layer fitting and excluded single layer case are included to consider and then determine a reliable range. In order to check the range, the mean position in several slices are evaluated. The points between red line are the result to establish a residual distribution. The Fig. 4.12 is the residual distribution after using the cut of position Y. It can be used to compare with Fig. 4.3 again. The standard deviation has a significant change in this figure.

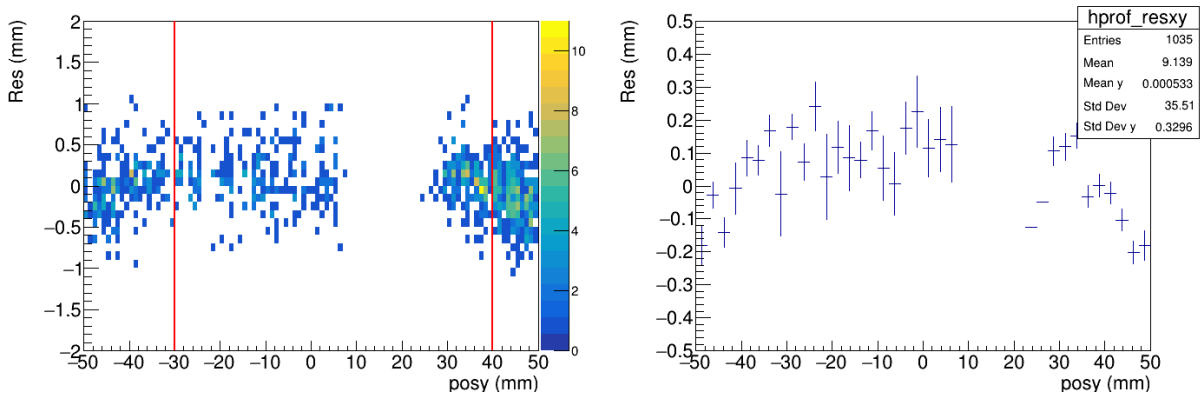

Figure 4.6: The local position Y versus residual X in GTR100 for all layer fitting case

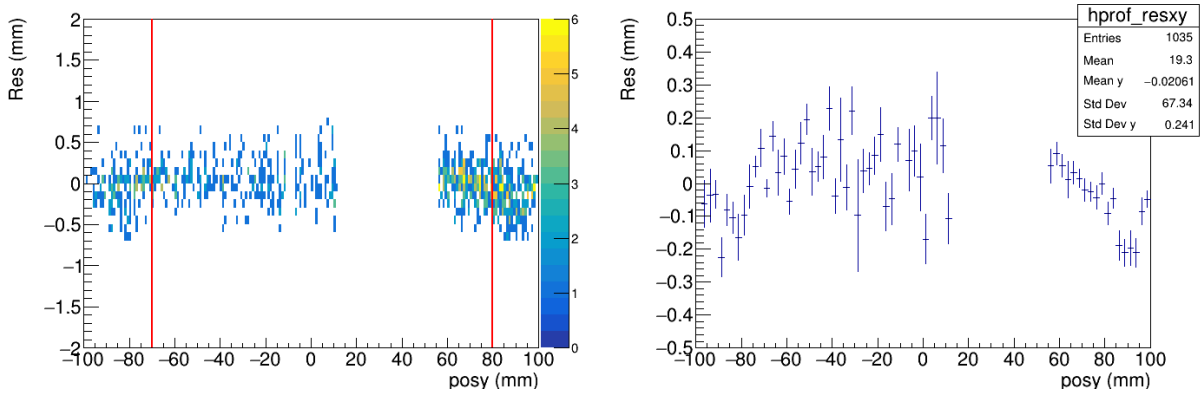

Figure 4.7: The local position Y versus residual X in GTR200 for all layer fitting case

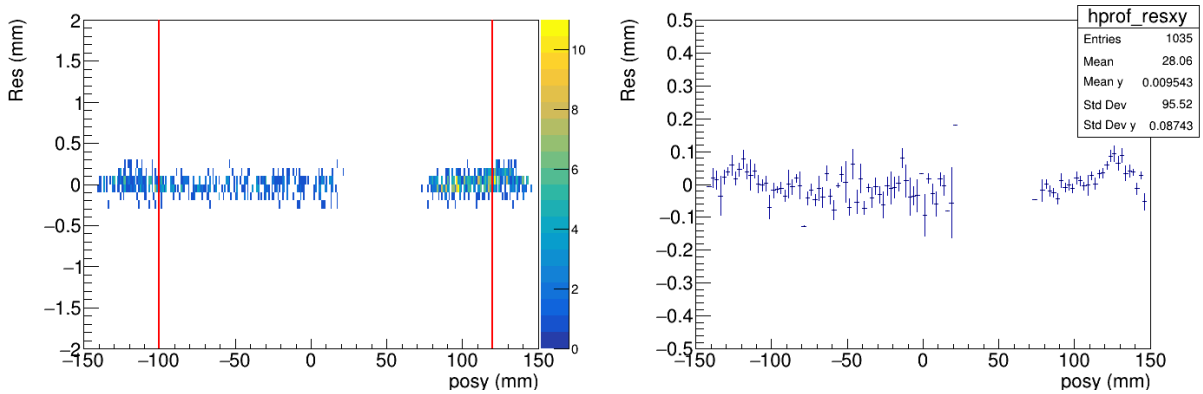

Figure 4.8: The local position Y versus residual X in GTR300 for all layer fitting case

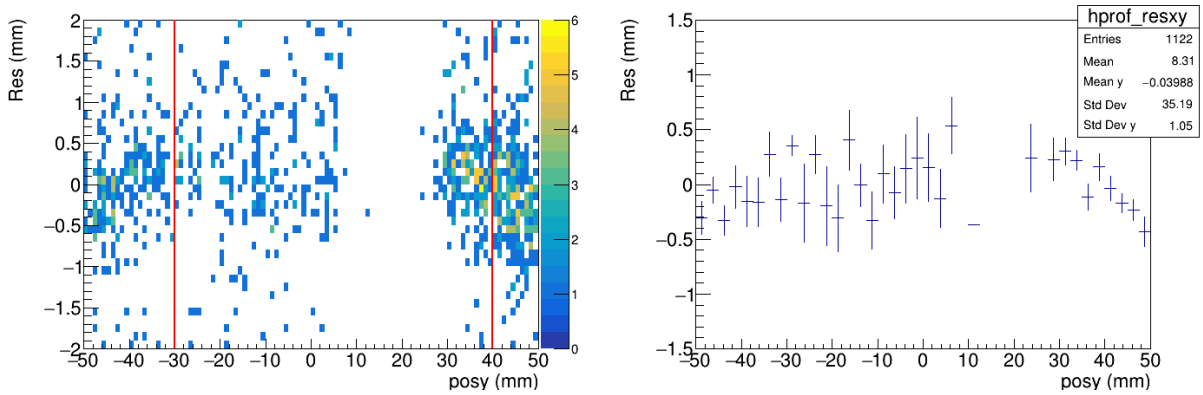

Figure 4.9: The local position Y versus residual X in GTR100 for excluded single layer case

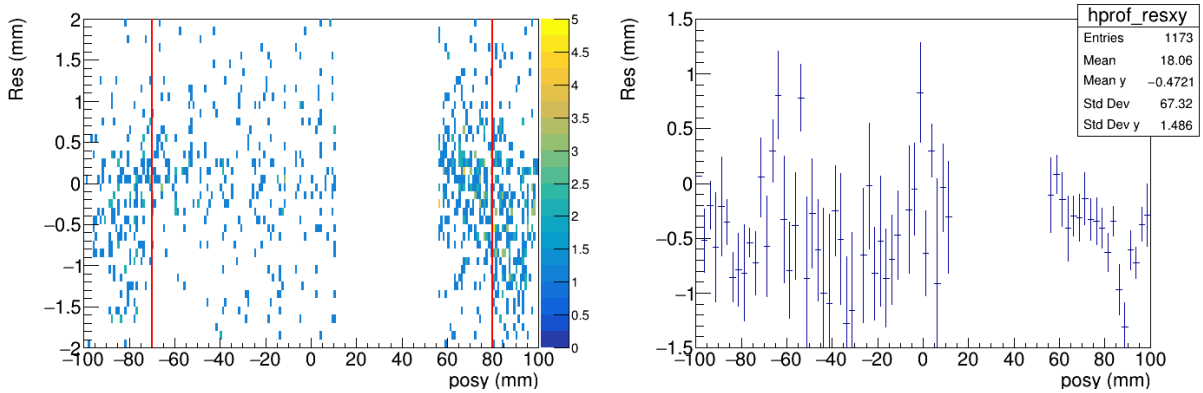

Figure 4.10: The local position Y versus residual X in GTR200 for excluded single layer case

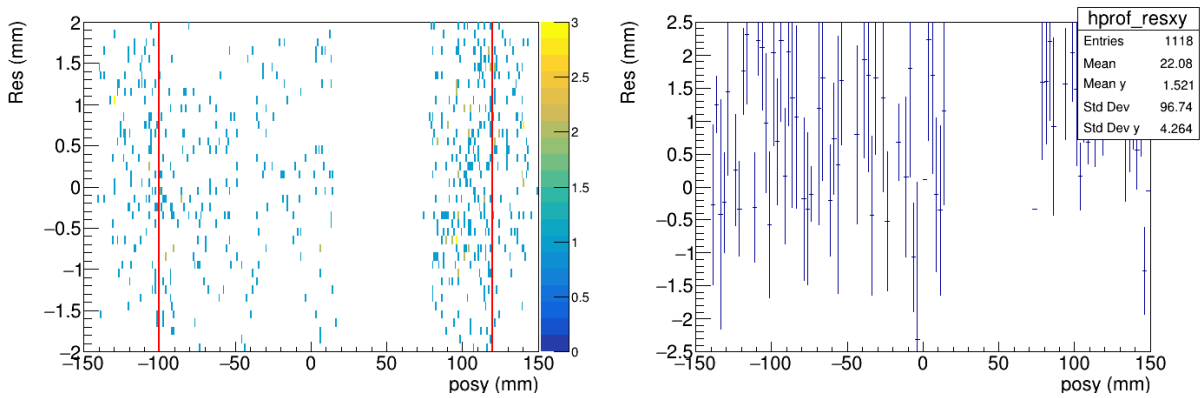

Figure 4.11: The local position Y versus residual X in GTR300 for excluded single layer case

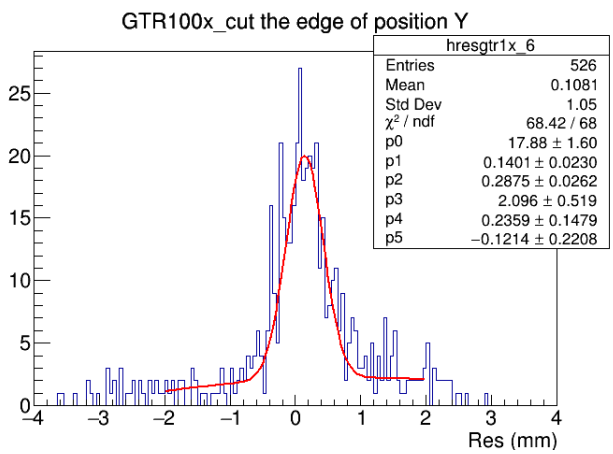

Figure 4.12: The residual distribution of GTR100x with using the cut of local position of Y direction

After trying different combination of cut condition, finally, the cut condition of position resolution used in the thesis are as fixed as : (1)Fundamental cuts, (2)HBD association, the ADC and residual of HBD, (3)traversing the same module, (4)cut of local position of Y direction. Other cuts like LG association and other GTRs' residual cut do not use in the analysis. The standard deviation of all layer fitting and excluded single layer with these cuts will be shown in final section of this chapter.

4.3 Efficiency

The detector efficiency is defined as a ratio of the number of tracks with associated hits to number of tracks. It should be evaluated after getting the result of position resolution because the range of hit finding is based on the $3\sigma_{resolution}$. If the setting of range is much tighter than 3σ, there may be not hit can be found and it causes the efficiency is underestimated. Oppositely, if we don't confine or use the coarse range, the hit has nothing to do with track may also be included. In that case, the efficiency will be overestimated.

The work of efficiency starts with tracking finding where the hits of corresponding layer are removed. Fake hit candidates are inserted randomly in a layer which need to evaluate. They are used to avoid the track finding bias. Abnormal ADC value is assigned for these artificial hits so that they can be removed easily in the analysis. Then, track fitting is performed and information is recorded. After that, the analysis work is performed. Finally, the efficiency can be evaluated, as discussed in Section 4.5.

Fig. 4.13 is the schematic of forming a track with the HBD and LG association for the efficiency of GTR100. The green points are projected positions of a track at the detectors. The detectors with grey color mean that the hits aren't used in the track reconstruction. The red cross refers to the hit on the corresponding layer, to be checked if it exists around within the projected position within 3σ. The sigma is decided by the fitting result of the residual distribution of the corresponding layer of GTR. Fig. 4.14 is an example for showing how to define the range of 3σ for GTR100x layer.

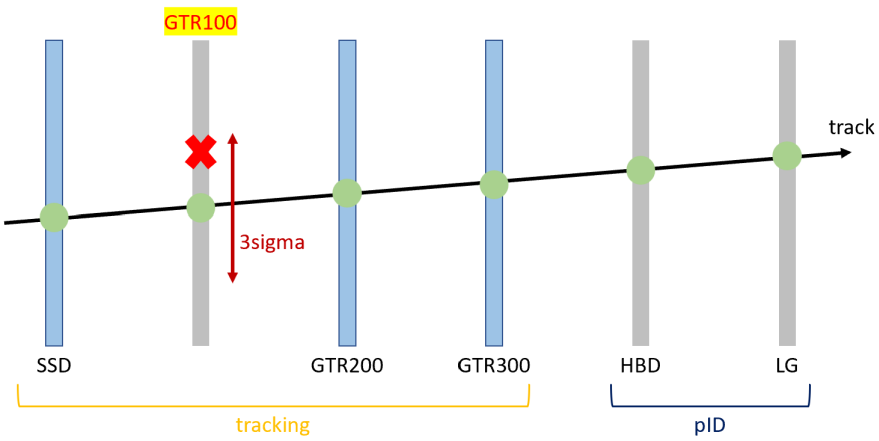

Figure 4.13: The schematic of track for the evaluation of efficiency

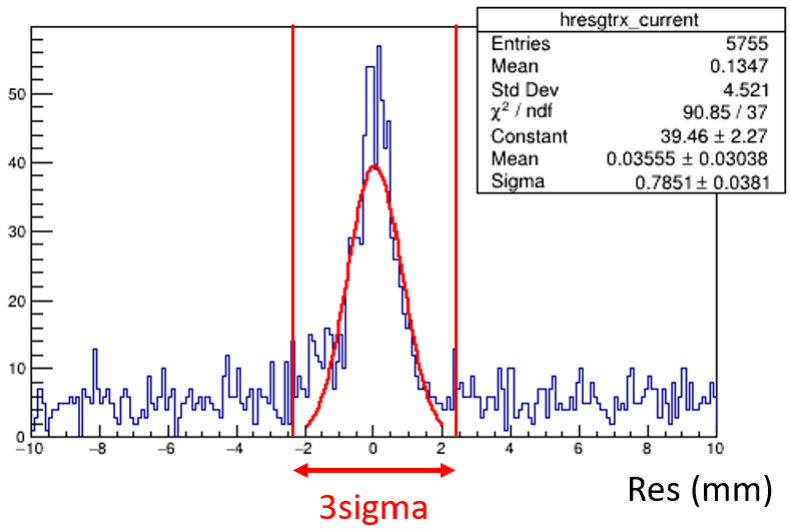

Figure 4.14: The residual distribution of GTR100x and the range of 3σ

4.4 Analysis of Efficiency

The efficiency analysis is similar to that of the resolution but some of contents are different. First difference is track candidate selection. Because the fake hits have been added in the fitting, there are fake track candidates reconstructed by them. For track candidates sharing the same hits on the other track detectors, the one with the best chi2 value is selected for efficiency study. The best-chi2 track candidate could be associated either with a true hit or a fake one. Second difference is cut condition, to determine a reliable track from many track candidates, HBD association and duplicate cut are essential. Here, the LG association is also used, so the track in the evaluation of efficiency must have a spatial dependence on LG. There is one more cut needed to used, which called the cut of dead area. Because some of strips did not work during the experiment, the 2D plot of hits in x and y direction is used to identify the dead area. The hits in x and y direction are recorded respectively, so all of combinations for each event are plotted. A dead strip will introduce a dead region over the whole range at the opposite direction. From Fig. 4.15, the dead areas are occurred at GTR200 and GTR300, which are white areas. So, if a track candidate enters the dead area of the corresponding layer, it is excluded.

There are two methods for evaluating the efficiency,

(1) Normal method
In this method, the efficiency is defined as follows,

$$Eff = \frac{N_{track \otimes hits}}{N_{track}}$$

where,
N_{track} : number of track, each track is selected by the cut condition of HBD, LG association and dead area.
$N_{track \otimes hits}$: number of tracks associated hits within the 3σ.

(2) Event mixing method

In order to calculate the efficiency precisely, meanwhile, reduce the potentially fake track in the N_{track} and the associated hit by noise in the $N_{track \otimes hits}$, the hits in the previous event are used to establish the residual distribution of background and then being subtracted in the efficiency calculation. So, the hits of LG are used to determine the background track and the hits of corresponding layer of GTR are calculated the background associated hits. Therefore, the equation of efficiency can be modified as,

$$Eff = \frac{N_{track \otimes hits} - N_{track \otimes hits\ previous}}{N_{track} - N_{track\ previous}}$$

where,

$N_{track\ previous}$: number of track in background, each track is selected by LG association which hits of LG in the previous event.

$N_{track \otimes hits\ previous}$: number of tracks with hits associated in background, check whether hits in the 3σ, the hits of GTR in the previous event.

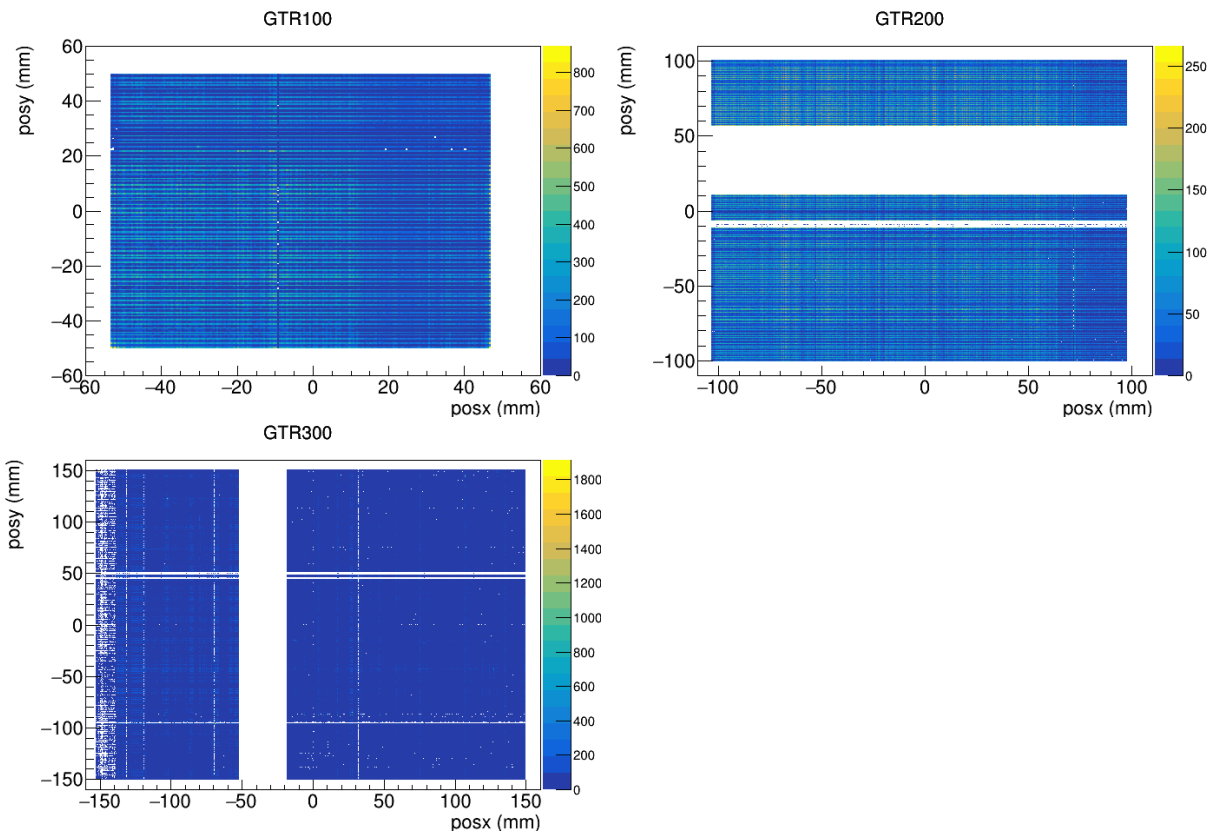

Figure 4.15: The 2D plots of x and y hits in three layers of GTR

4.5 Result of position resolution and efficiency

Position resolution

After using the cut conditions for the case of all layer fitting and excluded single layer, each final standard deviation of residual is determined. Fig. 4.16 and Fig. 4.17 show the residual distribution in the x and y direction for three layers of GTR. The standard deviations are extracted from the figures and shown in the Table. 4.3 and Table. 4.4. The position resolution of x and y direction with error bar are calculated. Here, the results are compared with (1) The result which released in the E16 Technical Design Report (E16-TDR), using the run0b data with a large statistic. (2) The parameters of weight of x and y direction are set in the track fitting.

Table 4.3: The position resolution of GTRs in x direction, unit : μm

	Residual of all layer	Residual of excluded single layer	resolution	E16-TDR	sigma
GTR100	194 ± 17	288 ± 26	236 ± 42	265 ± 8	300
GTR200	146 ± 18	363 ± 37	230 ± 52	252 ± 7	300
GTR300	68 ± 4	815 ± 139	235 ± 54	262 ± 6	300

Table 4.4: The position resolution of GTRs in y direction, unit : μm

	Residual of all layer	Residual of excluded single layer	resolution	E16-TDR	sigma
GTR100	200 ± 25	857 ± 61	414 ± 81	626 ± 56	1000
GTR200	323 ± 51	667 ± 61	464 ± 116	542 ± 20	1000
GTR300	250 ± 15	909 ± 70	477 ± 65	518 ± 27	1000

Compare the results from current study and E16-TDR, the position resolution in x direction for three layers of GTR are consistent. The results are also close to the parameter setting. So, the position resolution in x direction is successfully obtained. However, in y direction, the current results are smaller the previous consequence and parameter setting. The reduction of value may be caused by the cut of local y position. In the current study, the error bars are larger than which in E16-TDR. This issue can be resolved by increasing statistic possibly. However, the dependency of other data is not checked yet, so we cannot draw a conclusion. For the further study, the parameter setting in track reconstruction should be altered by the result of current study and then evaluating the position resolution again to check the difference. The determined position resolution can be considered as reliable if the input resolution parameter and the width of residual distribution are consistent with each other.

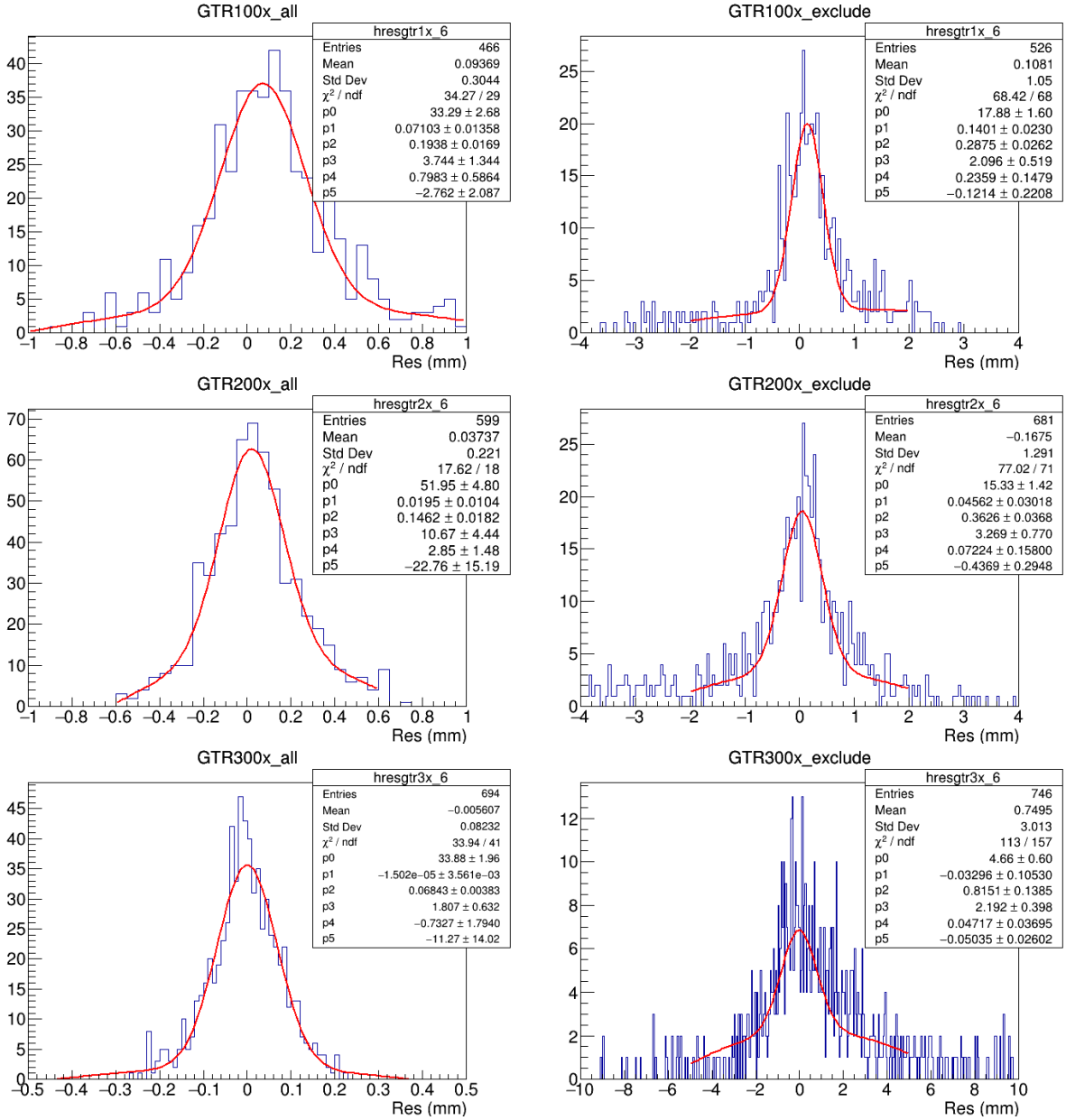

Figure 4.16: The residual distribution of all layer fitting and excluded single layer case in x direction

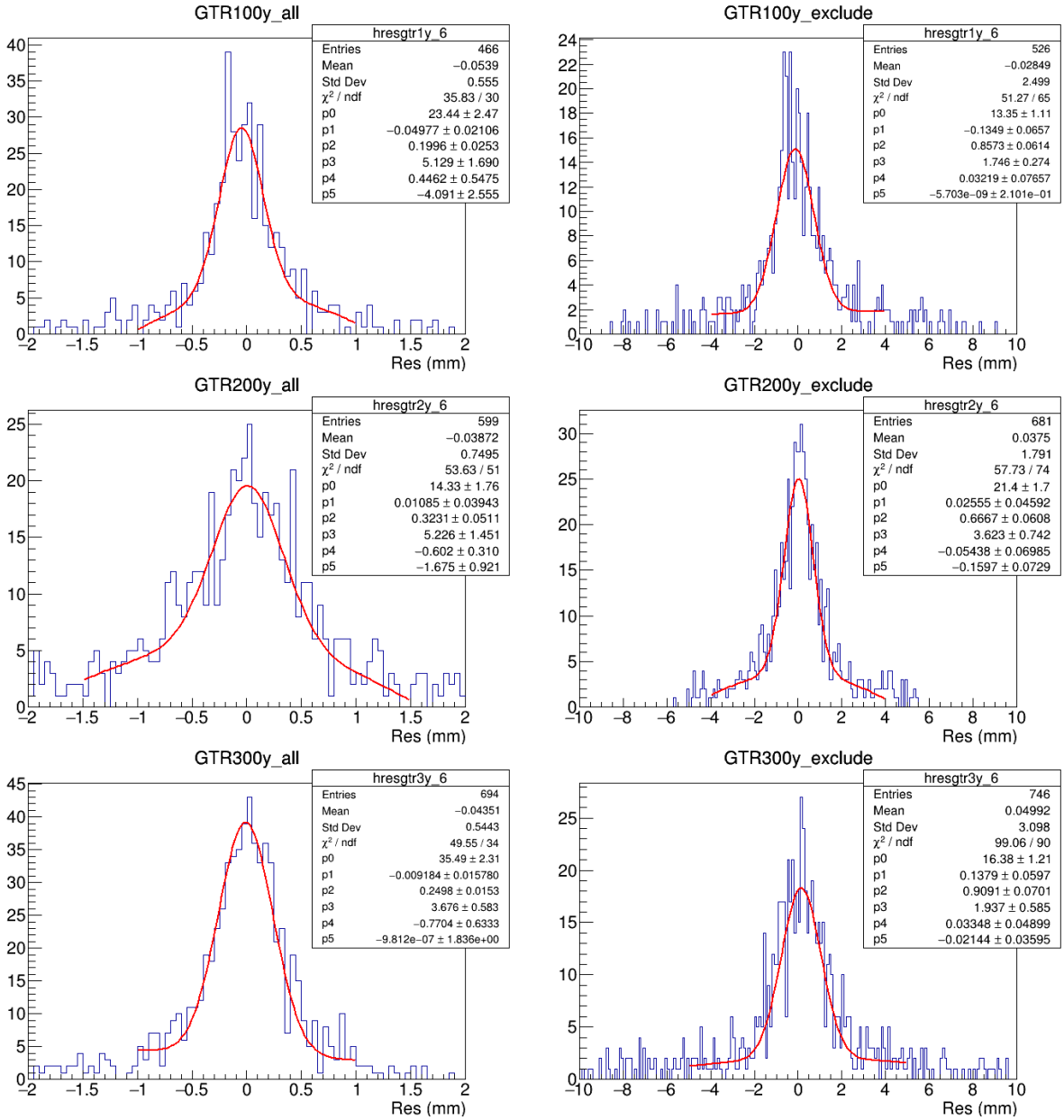

Figure 4.17: The residual distribution of all layer fitting and excluded single layer case in y direction

Efficiency

The results of efficiency are divided in x, y and x&y. In the denominator of equation, the N_{track} and $N_{track\ previous}$ are the same in these three cases for a layer of GTR. The difference is in the numerator, which refer to the number of track with hits associated in different direction. The calculation of efficiency x and efficiency y are independent, and their coincidence are used to evaluate the numerator of efficiency x&y. It is checked that if there are any hits in the x and y direction simultaneously.

The Table. 4.5 shows the efficiencies results in normal method and Table. 4.6 are results using the event mixing method. In normal method, we have a good efficiency in x direction but a low one in y direction. Another observation is that the consequence of effx&y is larger than the product of effx and effy, which means that the hits in x and y direction has some correlation. It is reasonable because if strip x has a hit, strip y should also have a hit. With the event mixing method, some efficiencies exceeded 1 and effx&y is higher than effx or effy. In order to understand the problem, going back to check every term in the equation is necessary.

Table 4.5: The efficiencies of GTRs in x, y and x&y in normal method

	effx [%]	effy [%]	effx&y [%]
GTR100	96.5	87.6	85.6
GTR200	95.4	76.6	75
GTR300	88.4	63.5	60.6

Table 4.6: The efficiencies of GTRs in x, y and x&y with using event mixing method

	effx [%]	effy [%]	effx&y [%]
GTR100	100.7	98.0	116.8
GTR200	100.5	99.8	107.1
GTR300	84.9	75.6	84.2

The compositions which used to evaluate efficiencies are shown in Table. 4.7 to Table. 4.9. As described previously, the N_{track} and $N_{track\ previous}$ are the same for one specific layer of GTR, independent of x or y planes. The $N_{track\otimes hits}$ and $N_{track\otimes hits\ previous}$ are also fine respectively. It is normal that the entries decrease when the coincidence of x and y is done. However, if $N_{track\otimes hits}$ minus $N_{track\otimes hits\ previous}$, the numerator result of eff x&y is larger than the others. This result is what make efficiency become strange. The current speculations to solve this issue are (1) modify the hit range of selection. (2) redefine the calculation of dummy hit of eff x&y. Because the problem is unsolved, the efficiencies are the results of the method in normal.

Table 4.7: the compositions which used to evaluate efficiencies of GTR100

	$N_{track \otimes hits}$	$N_{track \otimes hits\ previous}$	N_{track}	$N_{track\ previous}$	efficiency [%]
eff x	633	202	687	229	100.7
eff y	602	153	687	229	98.0
eff x&y	588	53	687	229	116.8

Table 4.8: the compositions which used to evaluate efficiencies of GTR200

	$N_{track \otimes hits}$	$N_{track \otimes hits\ previous}$	N_{track}	$N_{track\ previous}$	efficiency [%]
eff x	625	185	655	217	100.4
eff y	502	65	655	217	99.8
eff x&y	491	22	655	217	107.1

Table 4.9: the compositions which used to evaluate efficiencies of GTR300

	$N_{track \otimes hits}$	$N_{track \otimes hits\ previous}$	N_{track}	$N_{track\ previous}$	efficiency [%]
eff x	582	210	658	220	84.9
eff y	418	87	658	220	75.6
eff x&y	399	30	658	220	84.2

Chapter 5

Conclusion

The J-PARC E16 experiment aim to study the origin of hadron mass and the influence of chiral symmetry restoration in a finite density matter. The approach of experiment is the measurement of the mass spectra of light vector mesons produced at the finite nuclear density and reconstructed via the di-electron decay mode.

The GEM tracker is one of detector used to track charged particles. The goal of position resolution of GEM tracker is 100 μm. In order to achieve this result in the commission run, the calibration of tracking analysis is needed. In this thesis, the Lorentz angle and offset constant which are used for calculating a hit position for GTRs are fine-tuned to eliminate the dependency between tdc/posx/poxy and residual in x direction. After finishing the calibration, the dependency has a significant improvement in GTR100 and GTR200, the residual of each point is close to zero. However, for GTR300, the improvement is not clear. Although the updated result of GTR300 is still used, the precise reason needs further investigation.

With the updated parameters, the position resolution and efficiency are evaluated. For position resolution, the geometric mean method is used. The intrinsic position resolution is calculated by the standard deviation of all layer fitting and excluded single layer. The results of position resolution in x direction for three layers of GTR are 236 μm, 230 μm and 235 μm. All of them do not achieve the required resolution (100 μm), but consistent with the previous results. On the other hand, the results of position resolution in y direction are 414 μm, 464 μm and 477 μm. They are much smaller than the weight set in track reconstruction. To check the current results are reliable, altering the parameters and then running the track fitting again is necessary but it is not done.

For efficiency, the event mixing method is used to reduce the background. Unfortunately, the efficiency may exceed one and x&y term is larger than one direction term. So the event mixing method is fail in evaluating efficiency at this moment. The results of efficiency x are 96.5, 95.4 and 88.4 percentage. The results of efficiency y are 87.6, 76.6 and 63.5 percentage. The results of efficiency x&y are 85.6, 75 and 60.6 percentage.

The analysis in this thesis is performed for the module 106 using a single run data. In the future, the same calibration step could be applied to the other modules, hopefully with good enough statistic.

Appendix A

Information of analysis work

The source and analysis files are located at server "ccjbox6"

There are three important directories under the "/ccj/u/wangph/Documents", called
"ANA_calib" - the directory for calibration work
"ANA_resolution" - the directory for position resolution analysis
"ANA_efficiency" - the directory for efficiency analysis

In each directory, the source and header files are put at "E16DST1", there are several files need to be modified for calibration work and analysis.
For study 2, the changing of drift velocity and time should be done in the following files :
src/track/E16ANA_TrackCandidate.cc
src/GTR/E16ANA_GTRStripAnalyzer.cc
src/GTR/E16ANA_GTRAnalyzer2.cc
src/GTR/E16ANA_GTRAnalyzerMaker.cc
include/track/E16ANA_TrackCandidate.hh
include/GTR/E16ANA_GTRStripAnalyzer.h
include/GTR/E16ANA_GTRAnalyzer2.h

For study 3, the changing of Lorentz angle and offset constant should be done in the following files :
(include the above modification)
include/E16DST_DST1Constant.hh
include/track/E16ANA_TrackCandidate.hh

The process of finding new parameters could be helped by the script, for example,
/ccj/u/wangph/Documents/ANA_calib/work/search_LorentzAngleA/GTR1/exe_322_run1.sh

For position resolution analysis :
(include the above modification)
include/track/E16ANA_TrackParameter.hh

For efficiency analysis :
(include the above modification)
src/E16DST_DST1GTRFactory.cc
src/track/E16ANA_TrackCandidate.cc

The executable file used to produce a Rootfile is "dst0_to_dst1_trigger_check"
The files for analyzing the rootfiles are put at directories - "work*", which under each ANA_* directory.

The location of run30322 data,
/ccj/w/data06z/E16/Run0c/prod-1/dst0/all-calib/
the file names are "all-run030322*.dst0", with different number.

The location of run30464 data,
/ccj/w/data06z/E16/Run0c/prod-1/dst0/all-mag/
the file names are "all-run030464*.dst0", with different number.

Appendix B

The detail of correlation graphs

In correlation graphs (Fig3.9 $\sim$ Fig3.14), each point is obtained from the fitting result of residual distribution. These residual distributions are shown in the following link,

http://140.109.102.200/twiki/pub/JPARC/E16MC/pohung_thesis_appendix.pdf

These figures can help to check the fitting situation of each residual distribution. Actually, some of slice do not have a shape of gaussian due to the lack of statistic or in the edge. Here, four examples are taken to illustrate what happen on a point. The figure on left hand side will show the correlation graph and specified one of the points. Then the figure on right hand side will show its residual distribution.

1. Normal distribution
The residual distribution is extracted from the point which is the posx&mean correlation for study 3 in GTR200. The distribution has a significant signal with wide background. In order to get a precise result, the fitting function is used the gaussian with second order polynomial function.

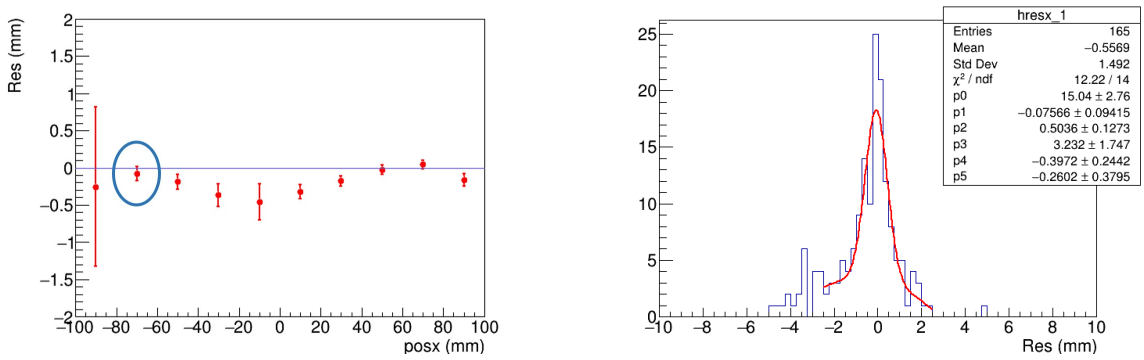

Figure B.1: The normal residual distribution in a slice

2. On the edge

The residual distribution is extracted from the point which is the posx&mean correlation for study 3 in GTR200. Usually, the entries are less than the other slice and it is hard to fit by gaussian, so the error bar becomes very large.

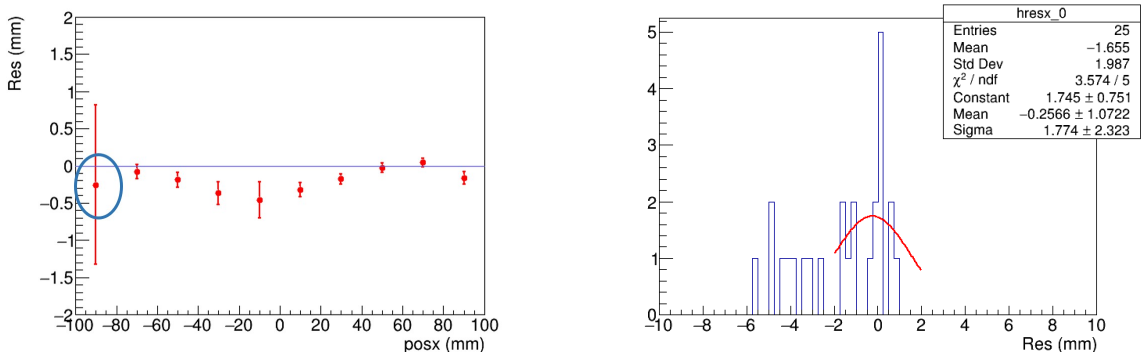

Figure B.2: The residual distribution of slice which on the edge

3. No entries

The residual distribution is extracted from the point which is the posy&mean correlation for study 3 in GTR200. Because of the dead area in the detector of y direction, there are no entries in the specified range.

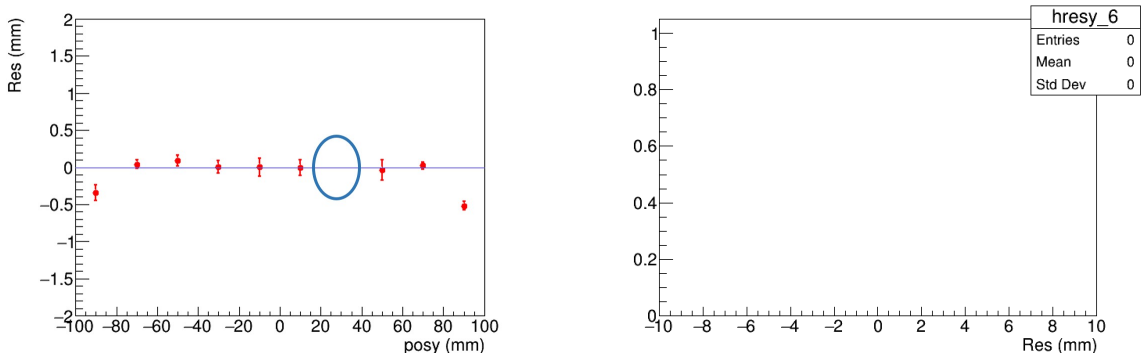

Figure B.3: A slice which does not have any entry

4. problem for GTR300

The residual distribution is extracted from the point which is the posx&mean correlation for study 3 in GTR300. In GTR300, many of distributions do not have a clear signal peak. Therefore, the fitting is not good for describing, which may cause the error bar becomes larger.

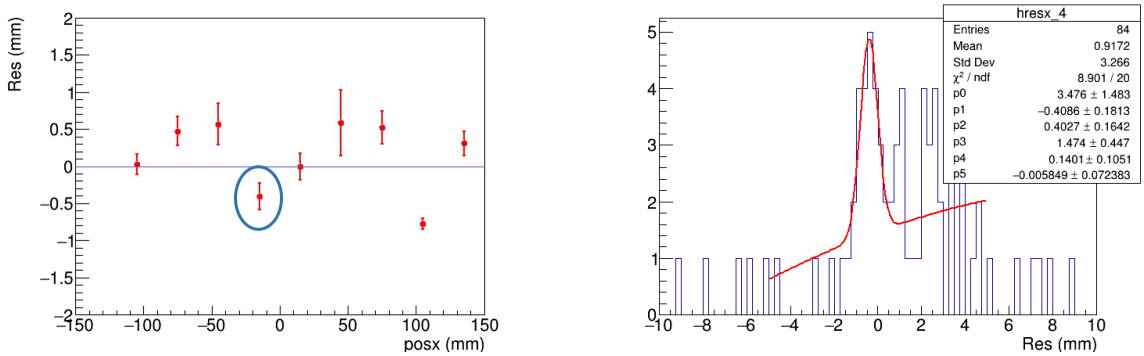

Figure B.4: The residual distribution of general situation in GTR300

Bibliography

[1] Michael E. Peskin. "Concepts of Elementary Particle Physics". (2019), pp. 217-223.

[2] David Tong. "Lectures on Gauge Theory - 5. Chiral Symmetry Breaking". http://www.damtp.cam.ac.uk/user/tong/gaugetheory/5chisb.pdf

[3] Michael E. Peskin and Daniel V. Schroeder. "An Introduction To Quantum Field Theory". (1995), pp. 667-671.

[4] H. Sazdjian. "Introduction to chiral symmetry in QCD". (2017), pp. 1-7.

[5] W. Weise. "Nuclear aspects of chiral symmetry. Nuclear Physics A". Vol. 553, pp. 59–72, (1993).

[6] G. E. Brown and Mannque Rho. "Scaling effective Lagrangians in a dense medium". Phys. Rev. Lett. 66, 2720, (1991).

[7] Tetsuo Hatsuda and Su Houng Lee. "QCD sum rules for vector mesons in the nuclear medium". Phys. Rev. C 46, R34 (1992).

[8] F. Klingl, N. Kaiser, and W. Weise. "Current correlation functions, QCD sum rules and vector mesons in baryonic matter". Nuclear Physics A, (1997).

[9] D. Adamov et al. "Modification of the ρ meson detected by low-mass electron–positron pairs in central Pb–Au collisions at 158A GeV/c". Physics Letters B 666, 425 (2008).

[10] S. Damjanovic. "NA60 results on the ρ spectral function in In-In collisions". Nuclear Physics A 783, 327 (2007).

[11] M. Naruki et al. "Experimental Signature of Medium Modifications for ρ and ω Mesons in the 12 GeV p+A Reactions". Phys. Rev. Lett. 96, (2006).

[12] M. H. Wood et al. "Light vector mesons in the nuclear medium". Phys. Rev. C 78, (2008).

[13] R.Muto, et al. "Evidence for In-Medium Modification of the ϕ Meson at Normal Nuclear Density". Physical Review Letters, (2007).

[14] S. Yokkaichi et al. "Proposal - Electron pair spectrometer at the J-PARC 50-GeV PS to explore the chiral symmetry in QCD". (2006).

[15] M. Ichikawa et al. "Commissioning Runs of J-PARC E16 Experiment". (2023).

[16] Facilities at J-PARC, https://j-parc.jp/c/en/facilities/index.html

[17] Accelerator facility, https://j-parc.jp/c/for-researchers/accelerators.html

[18] Website of J-PARC E16 experiment, https://ribf.riken.jp/~yokkaich/E16/E16-index.html

[19] Yuki Obara. "Development of the large GEM tracker and the trigger system for the J-PARC E16 experiment". Master's Thesis, The University of Tokyo, (2015).

[20] Tomoki Murakami. "Development and construction of GEM tracker system for the J-PARC E16 experiment". Master's Thesis, The University of Tokyo, (2020).

[21] Fabio Sauli. "Gaseous radiation detectors: Fundamentals and Applications". pp. 383-386.

[22] S. Yokkaichi et al. "Addendum to the J-PARC E16 Technical Design Report –for Run-1 approval–". (2022).

[23] Analysis results of Y. Morino about the calibration of GTR, http://140.109.102.200/twiki/pub/JPARC/E16MC/e16_ymorino_gtrcalib.pdf

[24] Claus Grupen and Boris Shwartz. "Particle Detectors Second Edition". (2008), pp. 43-49.

[25] Lia Lavezzi. "The new cylindrical GEM inner tracker of BESIII". (2018)

[26] A. Zhang1 and M. Hohlmann. "Accuracy of the geometric-mean method for determining spatial resolutions of tracking detectors in the presence of multiple Coulomb scattering". Journal of Instrumentation, (2016).

[27] T Alexopoulos et al. "Examining the Geometric Mean Method for the Extraction of Spatial Resolution". Journal of Instrumentation, (2014).